NAVAL POSTGRADUATE SCHOOL

MONTEREY, CALIFORNIA

THESIS

ANALYSIS OF POINT-SPREAD FUNCTION FOR IMAGING MOVING TARGETS FROM SCATTERED WAVES

by

Tan Lu Pin

December 2008

Thesis Advisor:	Brett H. Borden
Second Reader:	Donald L. Walters

Approved for public release; distribution is unlimited

THIS PAGE INTENTIONALLY LEFT BLANK

REPORT DOCUMENTATION PAGE			Form Approved OMB No. 0704-0188
Public reporting burden for this collection of information is estimated to average 1 hour per response, including the time for reviewing instruction, searching existing data sources, gathering and maintaining the data needed, and completing and reviewing the collection of information. Send comments regarding this burden estimate or any other aspect of this collection of information, including suggestions for reducing this burden, to Washington headquarters Services, Directorate for Information Operations and Reports, 1215 Jefferson Davis Highway, Suite 1204, Arlington, VA 22202-4302, and to the Office of Management and Budget, Paperwork Reduction Project (0704-0188) Washington DC 20503.			
1. AGENCY USE ONLY ***(Leave blank)***	**2. REPORT DATE** December 2008	**3. REPORT TYPE AND DATES COVERED** Master's Thesis	
4. TITLE AND SUBTITLE Analysis of Point-Spread Function for Imaging Moving Targets from Scattered Waves		**5. FUNDING NUMBERS**	
6. AUTHOR(S) Lu Pin Tan			
7. PERFORMING ORGANIZATION NAME(S) AND ADDRESS(ES) Naval Postgraduate School Monterey, CA 93943-5000		**8. PERFORMING ORGANIZATION REPORT NUMBER**	
9. SPONSORING /MONITORING AGENCY NAME(S) AND ADDRESS(ES) N/A		**10. SPONSORING/MONITORING AGENCY REPORT NUMBER**	
11. SUPPLEMENTARY NOTES The views expressed in this thesis are those of the author and do not reflect the official policy or position of the Department of Defense or the U.S. Government.			
12a. DISTRIBUTION / AVAILABILITY STATEMENT Approved for public release; distribution is unlimited		**12b. DISTRIBUTION CODE**	

13. ABSTRACT (maximum 200 words)

Radar imaging is an area of tremendous interest as radar-based systems are perhaps the only all-weather, long range remote sensing systems. However, radar's continued utility and application in wide-ranging areas is fundamentally dependent on the ability to produce high-quality, artifact-free imagery. To date, the use of radar to identify and image moving objects remains of great interest, and it is well known that motion in the scene gives rise to mispositioning or streaking when target motion is not addressed. Many techniques have been developed to handle moving objects, but these techniques make use of the *start-stop* approximation, in which a target in motion is assumed to be momentarily stationary while it is being interrogated by a radar pulse.

A new linearized imaging theory that combines the spatial, temporal and spectral aspects of scattered waves has been developed. This thesis studies the performance of this new imaging scheme via analysis of the point spread function. It is shown that the imaging PSF localizes, and is translation invariant in phase-space. It is also shown that the behavior of the imaging system is dependent on the aperture geometry and choice of radar waveforms transmitted.

14. SUBJECT TERMS Radar Imaging, Moving Targets, Point-Spread Function			**15. NUMBER OF PAGES** 81
			16. PRICE CODE
17. SECURITY CLASSIFICATION OF REPORT Unclassified	**18. SECURITY CLASSIFICATION OF THIS PAGE** Unclassified	**19. SECURITY CLASSIFICATION OF ABSTRACT** Unclassified	**20. LIMITATION OF ABSTRACT** UU

NSN 7540-01-280-5500 Standard Form 298 (Rev. 2-89)
Prescribed by ANSI Std. 239-18

THIS PAGE INTENTIONALLY LEFT BLANK

Approved for public release; distribution is unlimited

ANALYSIS OF POINT-SPREAD FUNCTION FOR IMAGING MOVING TARGETS FROM SCATTERED WAVES

Lu Pin Tan
Major, Republic of Singapore Navy
Bachelor of Engineering (EE), National University of Singapore, 1999

Submitted in partial fulfillment of the
requirements for the degree of

MASTER OF SCIENCE IN COMABT SYSTEMS SCIENCES AND TECHNOLOGY

from the

NAVAL POSTGRADUATE SCHOOL
December 2008

Author: Lu Pin Tan

Approved by: Brett Borden
Thesis Advisor

Donald Walters
Second Reader

James H. Luscombe
Chairman, Department of Physics

THIS PAGE INTENTIONALLY LEFT BLANK

ABSTRACT

Radar imaging is an area of tremendous interest as radar-based systems are perhaps the only all-weather, long range remote sensing systems. However, radar's continued utility and application in wide-ranging areas is fundamentally dependent on the ability to produce high-quality, artifact-free imagery. To date, the use of radar to identify and image moving objects remains of great interest, and it is well known that motion in the scene gives rise to mispositioning or streaking when target motion is not addressed. Many techniques have been developed to handle moving objects, but these techniques make use of the *start-stop* approximation, in which a target in motion is assumed to be momentarily stationary while it is being interrogated by a radar pulse.

A new linearized imaging theory that combines the spatial, temporal and spectral aspects of scattered waves has been developed. This thesis studies the performance of this new imaging scheme via analysis of the point spread function. It is shown that the imaging PSF localizes, and is translation invariant in phase-space. It is also shown that the behavior of the imaging system is dependent on the aperture geometry and choice of radar waveforms transmitted.

THIS PAGE INTENTIONALLY LEFT BLANK

TABLE OF CONTENTS

LIST OF FIGURES

THIS PAGE INTENTIONALLY LEFT BLANK

ACKNOWLEDGMENTS

The author is grateful to his thesis advisor, Professor Brett Borden, for introducing him to the fascinating world of radar imaging and generously sharing his knowledge. His ability to articulate key ideas in complex subjects made his lessons incredibly insightful and enjoyable. As an advisor, his faith and encouragement throughout the thesis work had been a constant pillar of strength and support. The author would also like to thank Professor Donald Walters, whose careful reading and many helpful comments contribute towards improving both the flow and clarity of this thesis. To my loving wife, Jaime, who was there every step of the way, and shared all the pain and joy in this endeavor. Finally to my two wonderful children, Kai Xin and Kai Rui – who I hope will grow up to love Physics and Mathematics; and my wonderful family patiently awaiting my return back in Singapore.

THIS PAGE INTENTIONALLY LEFT BLANK

I. INTRODUCTION

A. RADAR IMAGING

Sensor systems that can detect, locate and identify targets at great distances and in all kinds of weather have well-recognized utility. Radar-based systems are capable of performing such functions over long-range, all-weather and all-day (day or night) unlike many optical counterparts. This is because the wavelength of radar signals makes them relatively unaffected by atmospheric and weather-induced attenuation. Herein also lies the problem: image resolution depends upon signal wavelength. The resultant side effect is that resolution suffers and radar-based imaging will be fundamentally less effective compared to other systems based upon relatively shorter signal wavelengths. Nevertheless, radar waves scatter strongly from objects whose size is on the same order as the wavelength. This means that radar is sensitive to objects whose length scales range from centimeters to meters. Many objects of interest are in this range.

Many research and development efforts have been expended to improve the use of radar for imaging. It has been reported that resolution on the order of centimeters can be achieved with spotlight-mode operation [15]. While the developed techniques have been instrumental in making radar imaging a more viable application, the parallel advent of fast digital computers and leaps in computational prowess, have enabled practical systems to be fielded. This has generated great activity in areas such as interferometric synthetic aperture radar (SAR) and bistatic SAR, due to interest in operational concepts. The key to success in all of these applications is the ability to produce high-quality, artifact-free imagery.

B. IMAGE ARTIFACTS

The subject of radar (and radar imaging) has evolved considerably since the 1950s. Consequently, many implicit assumptions are embedded within current imaging techniques. These simplifications or system limitations are of interest as they are

frequently also responsible for the image artifacts discussed in the literature. The start-stop approximation is central to the thesis and holds the fundamental difference between the new imaging scheme developed in [2] and current techniques.

1. Scattering Model - Born Approximation

Historically, scattering models have been built upon a foundation which views targets as being composed of simple, non-interacting point scatterers. When the imaging scene consists of multiple targets, accounting for multiple scattering (in which waves bounce back and forth between the targets) can become extremely complex. For this reason, the 'weak scatterer' or Born approximation is typically invoked. A useful consequence is that the imaging problem becomes linear and more tractable.

However, the Born approximation may result in image artifacts as actual "multiple-scattered" waves are received later than expected from the single-scattering model. These waves are then interpreted as having come from a more distant target structure. In addition, increased capabilities in radar resolution and sensitivity and parallel advancements in computational technology have exposed the inadequacies of such simple scattering models. With the ability of radar systems to resolve and image the *components* (subscatterers) that lie *within* the support of a traditional target, it is inevitable that new radar target models that can describe these multiple scattering effects accurately (whether multiple targets or multiple components of a single target) are required. Current approaches typically utilize correction techniques to enhance imaging algorithms based on the low order 'weak scatterer' model.

2. Measurement Systems

There are inherent limitations in any data that are measured by radar systems. Such data are usually corrupted by noise and are always limited by bandwidth. Consequently, inducing unwanted image artifacts and reduced image resolution.

3. "Start-Stop" Approximation

The radar uncertainty principle bounds the accuracy with which time delay and frequency shift can be simultaneously estimated using a single pulse. This limitation may be mitigated by the use of follow-on pulses to further probe target characteristics. Most modern radars use a train of high range-resolution waveforms to enable pulse-to-pulse velocity estimation. Such waveforms allow the use of the *start-stop* approximation, which assumes that the target is stationary during the time the radar pulse illuminates the target, and moves only between pulses. When individual pulses are short, and targets of interest are small and move slowly compared to the speed of light, this is almost always a good approximation. Under these circumstances, good velocity estimates are obtained from the range-rate (two accurate range measurements, separated by a time interval). Unfortunately, *no* Doppler information is actually measured by the systems. Range and range-rate information are then used to form spatial images.

In order to achieve the necessary signal-to-noise ratio (by coherent integration), long pulse trains are required. Consequently, during the coherent processing interval, the stationary target assumption may no longer hold. Scatterers may move to different positions, and when they move beyond a resolution cell, the result is a blurred image.

C. MOTIVATION - IMAGING MOVING TARGETS

In recent years, a number of attempts to develop imaging techniques that can handle moving objects have been proposed. Space-time adaptive processing (STAP) is a signal processing technique that was originally developed for detecting slow-moving targets using airborne radars. STAP uses multiple-element antenna array, together with real-aperture imaging techniques to produce ground moving target indicator (GMTI) images [23]. This method described in [24] combines SAR (designed to image stationary scenes) and GMTI processing to develop new techniques for detecting slow-moving surface targets that exhibit start-stop maneuvers. The method described in [11] discusses the extension to non-sideways looking array radar.

The method described in [10] describes the concept of velocity synthetic aperture radar (VSAR). VSAR is a multi-element SAR system involving conventional processing to form an image at each element; except the image phases are preserved and compared to deduce target velocity. However, VSAR processing assumes that the scatterers remain in a single resolution cell throughout the integration time.

Time-frequency methods for signal analysis allow decomposition of the frequency spectrum of time-varying signals in shorter time-frames, and provide an added dimension for examining the dynamic behavior of the signal as it varies over time. The size and shape of the weighting window function can be altered to fit the specific analysis requirement for the signal. In recent years, further extension of this time-frequency method to ISAR has been advocated in the area of image generation, motion compensation and micro-Doppler target vibration studies [Refs. 8, 20 and 21]. Chen [20] has reportedly used the time-frequency transform (TFT) to construct inverse synthetic aperture radar (ISAR) images of targets with high rotation rate by helping to overcome the migration of individual scattering points from one range cell to another.

However, all of these techniques rely on making the approximation that a target in motion is assumed to be momentarily stationary while interrogated by a radar pulse. It is apparent that the utility of an imaging approach that can accommodate target motion during the imaging process. This constitutes the focus of the thesis.

D. OBJECTIVE

The objective of this thesis is to study a linearized imaging theory developed by *Cheney, Borden* [2] for an imaging region containing moving objects. The physics involved, and the approach for addressing image artifacts common to targets moving in an *unknown* fashion will be discussed. Analysis of the corresponding point-spread function will be carried out to examine the localization in phase-space (position-velocity). The behavior (position, and velocity resolution) of the imaging system will also be examined under different aperture geometries and transmitted waveforms.

E. THESIS ORGANIZATION

The thesis is organized in the following manner:

Chapter II serves to develop the appropriate radar imaging theory by looking at the basic building blocks necessary for imaging – radar operating principle, scattering models, correlation reception – and how these components translate to imagery. Finally, the thesis includes an overview of the inverse nature of the radar imaging problem to provide better appreciation of issues pertaining to practical measurement systems and how information is extracted from measurements to obtain the best estimates of the target object.

Chapter III applies the concepts put forth in Chapter II to the imaging scenario. The discussion here is based on the work of Cheney, Borden [2] in imaging moving targets from scattered waves. The effect of multiple moving targets on the scattering model is described. The approximations invoked, specifically slow-moving, narrow-band and far-field, will be examined. A scattering model to be used in the simulation program will be presented.

Chapter IV discusses the radar ambiguity function, and the relationship between estimation errors and the transmitted waveform. Particular emphasis will be given to image quality analysis and the derivation of the point-spread function to quantify the performance of the imaging scheme developed in Chapter III.

Chapter V examines further implications of the transmitted waveform through the pulse compression perspective. In particular, the Chirp signal is discussed.

To demonstrate the behavior of the imaging scheme, a simple simulation program is developed for modeling the point-spread function. Chapter VI discusses the results of the simulation, specifically the effect of different aperture geometries and transmitted waveform characteristics. It also concludes and summarizes the major findings of the thesis work and provides recommendations for future work.

THIS PAGE INTENTIONALLY LEFT BLANK

II. IMAGING THEORY

Prior to deriving the radar data model for imaging moving targets, Chapter II examines the formation of spatial images. It begins by examining the physics behind extracting range and range-rate (Doppler shift) information by a radar system. A simple range-Doppler imaging example is presented. The chapter concludes with a brief look at the inverse nature of the imaging problem and characteristics of measurement systems, and from there some of the issues/challenges pertaining to radar imaging.

A. BASIC RADAR PRINCIPLES

Most fielded radar systems are pulsed systems, as opposed to stepped-frequency systems. Radar systems measure the strength of the backscattered field and the round trip delay time of transmitted signal pulse reflected from distant objects. Since the radar pulse travels at the speed of light, it is practical to use the measured time delay for the round trip to determine the range to the reflecting object. This is the basic principle of radar theory and we can determine the range R from $R = c\tau / 2$ (where τ is the round trip time delay).

Several concepts will be useful in appreciating how radar signals convey information for the imaging output. The first is concerned with the kind of signals that a radar uses to generate the waveforms it transmits. Radar signals are real-valued functions of time but it is convenient to express the waveforms as complex-valued functions. Radar systems are able to measure these signals (in both amplitude and phase) as functions of time. The imaginary part of the complex signal provides the phase of the waveform revealing considerable information about the target.

Radar waves are electromagnetic waves governed by Maxwell's equations. The waveforms generated from radar signals satisfy the wave equation and the radiation condition. These properties 'code' the echo (transmitted wave scattered from a radar target) waveform with important target specific information such as range, speed and bearing.

The resolution in the down-range direction is governed by the pulse width, and correspondingly its pulse bandwidth. Typical carrier frequency operation bands occur within the low attenuation atmospheric windows ~ 1-40 GHz. The frequency band of the system, in practice, signifies that radar signals are always of finite duration. Intuitively, a higher bandwidth will imply finer resolution for imagery in the range direction. More about the concept of "resolution" will be addressed in Chapter IV.

B. SCATTERING OF ELECTROMAGNETIC WAVES

Understanding the behavior of electromagnetic waves, specifically propagation and scattering of these waves, is essential to appreciating the information that can be extracted from the transmitted signals. The next two sections will elaborate this further.

The discussion of [18] describes a simple one-dimensional scattering model for a moving PEC[1] plate in free space (a good approximation for typical radar wave propagation). An elementary consequence of Maxwell's equations is that an electromagnetic wave (in the far-field) must have the *electric field* $\vec{E}$, *magnetic field* $\vec{H}$ and *wave vector* (direction of wave propagation) $\hat{k}$ mutually perpendicular. For the transmitted wave with field components orthogonal to the x direction (i.e. in the y-z plane), the boundary condition on the PEC results in the following relationship between scattered and transmitted electric field:

$$\vec{E}_{scatt}\, g(t + R(t)/c) = -\vec{E}_{inc}\, f(t - R(t)/c)$$

where the scattered field consists of a left-travelling wave (in the negative x direction). The position of the moving plate is given by $R(t)$. Assuming for simplicity that the plate is undergoing linear motion[2] (with velocity v in the x-direction), so that

[1] A perfect electrical conductor (PEC) allows the charges to move freely and instantaneously in response to a field; consequently the fields inside a PEC are zero. The resulting boundary conditions are: the tangential components of the electric field must be zero; and the tangential components of the magnetic field are related to currents flowing on the surface of the PEC.

[2] Even if the motion is not linear, the linear expression $R(t) = x+vt$ can be considered to be the first two terms in a Taylor expansion that is valid for small t (i.e., for short pulses).

$R(t) = x + vt\Big|_{x=R(\text{at boundary})}$ and making use of the substitution $u = t + R(t)/c$, we can solve for *t* in terms of *u* (at the boundary):

$$t = \frac{u - R/c}{1 + v/c}$$

and obtain the expression for the scattered field

$$\vec{E}_{scatt}\, g(t + R(t)/c) = -\vec{E}_{inc}\, f\left[\alpha(t + x/c - R/c) - R/c\right] \tag{2.1}$$

where α is the Doppler scale factor

$$\alpha = \frac{1 - v/c}{1 + v/c} \tag{2.2}$$

For a transmitted field consisting of a signal waveform $s(t)$ mixed with a carrier wave $\cos(\omega_0 t)$, the scattered signal received at the antenna $(x = 0)$ is

$$p_{rec}(t) \approx s(t - 2R/c)\cos\left(\omega_0\left[(1 - 2v/c)(t - R/c) - R/c\right]\right) \tag{2.3}$$

We have used the fact that $s(t)$ is slowly varying to approximate the argument $\alpha(t - R/c) - R/c$ by $t - 2R/c$, and also the fact that for a scatterer moving slowly, so that υ/c is small. In addition, we can expand the denominator of Equation (2.2) in a geometric series and approximate α by $1 - 2v/c$. The multiplier of *t* in the argument of the cosine function, is the carrier frequency (relative to the transmitted carrier frequency) shifted by an amount

$$\upsilon = -\frac{2v}{c}\omega_0 \tag{2.4}$$

This is the Doppler shift. As in the stationary scatterer case, the received signal is time-delayed, but here it is also a Doppler-shifted version of the transmitted signal.

C. CORRELATION RECEPTION - RADAR DATA MODEL

Detection of signals in noise is fundamental to radar operations. A radar *detects the presence* of an echo signal reflected from a target and *extracts information* about the

target for uses such as imaging. The conservation of energy requires that the wave intensity from a finite-sized antenna decreases in strength as the inverse square of the distance. Consequently, the round trip power of the signal received by the same antenna for small targets decays by a factor of $1/R^4$ relative to the signal that was transmitted. For typical radar operational distances, the received power can be as low as 10^{-18} Watts consequently. Thermal noise in the receiver presents a problem for target detection, and a greater problem for image formation.

While increasing the power of the transmitter (or pulse integration) can help increase the signal-to-noise ratio (SNR), there are practical limits to relying solely on these approaches. Key amongst these limits is the decrease in maximum unambiguous range, and also the fact that targets move during data collection for pulse integration, altering the phase of the scattered field. It should be pointed out that the ensuing discussion is premised on the correlation comparison being performed coherently such that the phase of the transmission signal is preserved in the reference signal.

In practice, a solution involves transmitting long *coded* pulses, together with appropriate signal processing techniques called *matched filtering* or *correlation reception*. This is known as pulse compression (see Chapter V). The correlation receiver (or matched filter) is an important example of a radar signal processor for detection of desired signals. The output of the matched filter is the cross-correlation function of the received signal and the expected received signal (which is related to the transmitted signal). Hence, the mathematical equivalence between the correlation receiver and the matched filter receiver, and it is possible to implement the matched filter as a correlation process.

A radar obtains information about a target by comparing the received echo signal with the signal that was transmitted. Correlation reception presents an intuitive approach to develop the standard radar data model used in imaging. The signal processing problem is that of optimal detection in additive noise. Assuming Gaussian noise statistics, maximum likelihood processing (conditioned on the measured signal $s_{rec}(t)$) selects the best guess estimate for the radar signal associated with the field reflected from a target

$s_{scatt}(t)$ that maximizes the conditional probability. Reference [19] shows that such processing (averaged over all time) reduces to finding the function $s_{scatt}(t)$ that minimizes

$$\int_{-\infty}^{\infty} \left|s_{rec}(t')\right|^2 dt' + \int_{-\infty}^{\infty} \left|s_{scatt}(t')\right|^2 dt' - 2\,\mathrm{Re}\int_{-\infty}^{\infty} s_{rec}(t')s_{scatt}^{*}(t')dt' \tag{2.5}$$

The objective is to determine $s_{scatt}(t)$ from the random measurements of $s_{rec}(t)$. The first two terms are system-scenario specific. Searching for the best minimizing function hinges on the last term and can be made more efficient by restricting the search to a few parameters derived from some model. In this case, the natural model is based on the scattering interaction between the interrogating field and the target. If $s_{inc}(t)$ denotes an incident pulse transmitted by the radar, then the linear radar (weak-scatterer) scattering model follows by superposition

$$s_{scatt}(t) = \iint_{-\infty}^{\infty} \rho(\upsilon,\tau)s_{inc}(t-\tau)e^{i\upsilon(t-\tau)}d\tau d\upsilon \tag{2.6}$$

where $\rho(\upsilon,\tau)$ is the target reflectivity density for a radar system that measures two parameters (range and radial velocity). This reflectivity density is defined in such a way that $\rho(\upsilon,\tau)d\tau d\upsilon$ is proportional to the field reflected from the target at range between $c\tau/2$ and $c(\tau+d\tau)/2$ with Doppler shift between υ and $\upsilon+d\upsilon$.

From Equation (2.6), the scattered field is naturally modeled by the two parameters τ and υ. The simplified search space will be parameterized by the time shift τ and the frequency shift υ. Considering the last term of Equation (2.5), and maximizing for all τ, υ in the scattered model, the correlation integral is

$$\eta(\upsilon,\tau) = \int_{-\infty}^{\infty} s_{rec}(t')s_{inc}^{*}(t'-\tau)e^{-i\upsilon(t'-\tau)}dt' \tag{2.7}$$

The correlation integral seeks out the component of received signal that "matches" the time-delayed, frequency-shifted version of the transmitted signal. Unlike signals will be suppressed consequently; correlation receivers attempt to find the τ and υ that

maximize the real part of Equation (2.7). The expected output of the correlation receivers is obtained by substituting Equation (2.6) into the correlation integral of Equation (2.7)

$$\eta(\upsilon,\tau) = \iiint_{-\infty}^{\infty} \rho(\upsilon',\tau') s_{inc}(t'-\tau) s_{inc}^{*}(t'-\tau') e^{i\upsilon(t'-\tau)} e^{-i\upsilon(t'-\tau')} dt' d\tau' d\upsilon' \tag{2.8}$$

Recall that the signal-processing problem was detection of signals in noise, hence the received data $s_{rec}(t)$ consists of both the scattered signal and a random noise component. The correlation noise term, which is the correlation integral between random noise and the time-delayed, frequency-shifted version of the transmitted signal, has been dropped from Equation (2.8). The correlation noise term which measures how well the scattered signal matched the random noise will usually be small for coherent systems. Rearranging Equation (2.8),

$$\eta(\upsilon,\tau) = \iint_{-\infty}^{\infty} \rho(\upsilon',\tau') \chi(\upsilon-\upsilon',\tau-\tau') e^{i\frac{1}{2}(\upsilon+\upsilon')(\tau-\tau')} d\tau' d\upsilon' \tag{2.9}$$

where

$$\chi(\upsilon,\tau) = \int_{-\infty}^{\infty} s_{inc}(t'-\frac{1}{2}\tau) s_{inc}^{*}(t'+\frac{1}{2}\tau) e^{i\upsilon t'} dt' \tag{2.10}$$

Equation (2.9) is the standard radar data model and expresses the output of the correlation receiver as the convolution of ρ and χ (up to a phase factor). The function $\chi(\upsilon,\tau)$ defined by Equation (2.10) is the radar ambiguity function. Radar imaging is closely related to the radar ambiguity function that characterizes the accuracy that the target position and radial velocity are estimated from the radar data (see Chapter IV).

D. ONE-DIMENSIONAL (HIGH RANGE RESOLUTION) IMAGING

One-dimensional imaging involves the generation of range profiles, which can be used to articulate target substructure. For high range resolution (HRR) techniques, the transmitted pulse's instantaneous range resolution is smaller than that of the target, and as it sweeps across the target it sequentially excites the target's scattering subelements which re-radiate energy back to the receiver. When these scattering subelements are non-

interacting and point-like, the scattered pulse will be a sum of damped and blurred images of the incident pulse, which are shifted by time delays that are proportional to the subelement's range [1]. Figure 1 shows an example of one-dimensional images created by HRR radar systems. It can be observed that the profile displays additional peaks outside of the target support, clear evidence of the problem associated with a single, non-interacting scatterer approximation.

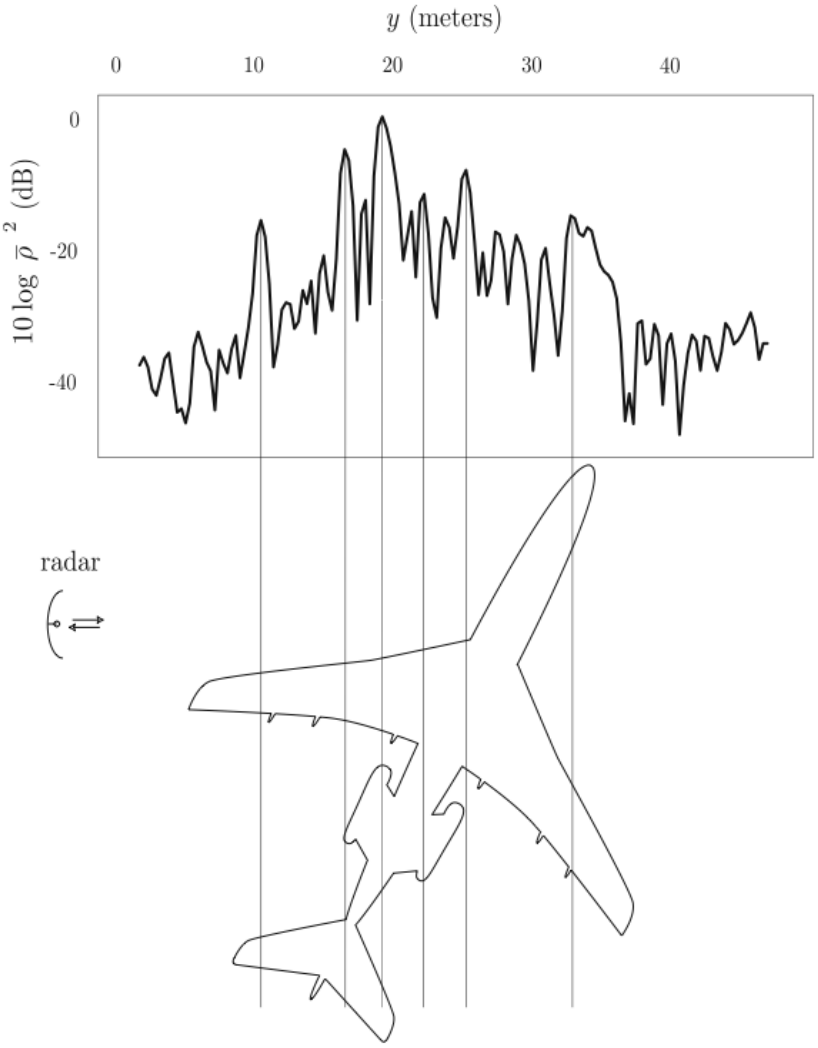

Figure 1. Example of a range profile from a B-727 jetliner. The top view (with orientation at time of measurement) is displayed beneath [1].

The signal received from a distribution of non-interacting, stationary targets can be modeled as

$$s_{rec}(t) = \int_{-\infty}^{\infty} \rho(\tau') s_{inc}(t - \tau') d\tau' + n(t) \tag{2.11}$$

where $n(t)$ represents an additive and random noise term. Application of a matched filter to obtain the radar data model used for imaging

$$\eta(\tau) = \int_{-\infty}^{\infty} s_{rec}(t') s_{inc}^{*}(t' - \tau) dt' = \int_{-\infty}^{\infty} s_{inc}^{*}(t' - \tau) \int_{-\infty}^{\infty} \rho(\tau') s_{inc}(t' - \tau') d\tau' dt' \quad + \quad \text{noise term}$$

$$= \iint_{-\infty}^{\infty} s_{inc}^{*}(t' - \tau) s_{inc}(t' - \tau') dt' \rho(\tau') d\tau' \quad + \quad \text{noise term}$$

Making the substitution $t'' = t' - \tau'$, and neglecting the noise term (negligible with matched filtering) gives

$$\eta(\tau) = \int_{-\infty}^{\infty} \chi(\tau - \tau') \rho(\tau') d\tau' \tag{2.12}$$

where χ is the autocorrelation

$$\chi(\tau) = \int_{-\infty}^{\infty} s^{*}(t'' - \tau) s(t'') dt'' = \int_{-\infty}^{\infty} s^{*}(t') s(t' + \tau) dt' \tag{2.13}$$

Equation (2.12) represents a one-dimensional image and shows how the true distribution ρ is related to the radar data model. The image is the convolution of ρ with χ, which in high-range resolution (HRR) imaging is also commonly referred to as the *point-spread function* (PSF). The point spread function obtains its name from the fact that if ρ consists of a single point $\delta(t)$, then the image is $\eta(t) = \int \chi(t - t') \delta(t') dt' = \chi(t)$. Thus, χ quantifies the degree to which a single point appears spread out in the HRR image.

The down-range profile can be affected by a variety of factors such as target aspect angle, position of the scatterers or masking of scatterers by other parts of the target. Additionally, while the use of short pulses enhances the resolution, it concurrently

leads to large bandwidth requirements. Wide bandwidth can increase system complexity and increase the likelihood of interference from other emitters in the electromagnetic spectrum. A short-pulse waveform also provides less accurate radial velocity measurement, a natural consequence from the properties of the radar ambiguity function (more details on radar resolution and the ambiguity function in Chapter III). An important implementation limitation to highlight for practical radar applications is the required high peak power to transmit short pulses over long ranges. High peak power transmission can be problematic, especially at high frequencies (due to the small waveguide dimensions and the small area of the anodes of the microwave sources).

Radar target recognition using only range profiles has limited applications. This is because a range profile will not be able to distinguish cross-range target structures. All scatterers located at the same distance from the radar will reflect energy back to the radar with the same time delay. Hence, when the radar illuminates many distinct targets at any instant, meaningful interpretation of on-scene target (multiple) disposition cannot be derived based on a set (single) of range-only data.

E. TWO-DIMENSIONAL IMAGING

For more effective target interpretation, additional information is needed on top of the range profile. This information can be in the form of high-resolution cross-range profile, Doppler profile, or simply the "triangulation" of range profiles.

As a simple illustration for extension of the radar imaging concept to two dimensions, "triangulation" of different sets of range profiles will be examined (Figures 2 and 3). This approach enables the determination of cross-range target structure while using only HRR radar systems and relies on collecting multiple sets of range profiles from different target orientations, processing them, and subsequently synthesizing a two-dimensional image.

Consider a set of three point targets with the radar located at the same distance from targets 2 and 3 (see Figure 2). When the geometry is oriented as shown, the return echo will only indicate two targets. Hence, ambiguity exists when targets lie along the bands of constant range from the radar.

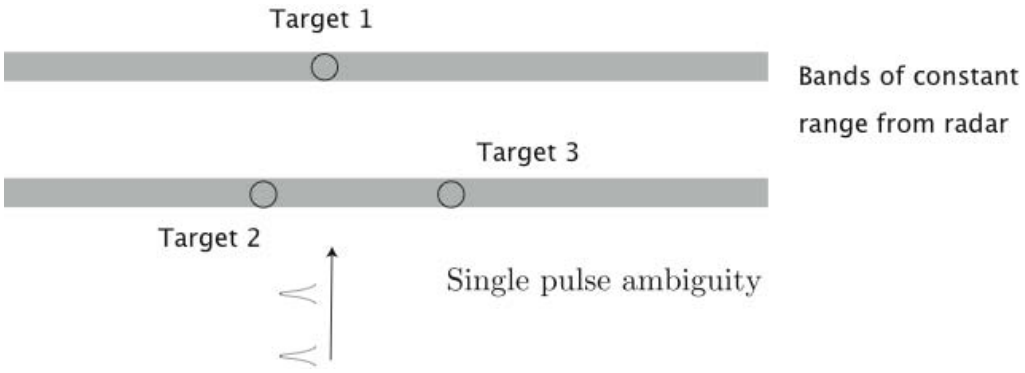

Figure 2. Ambiguous scenario from a single radar pulse [19].

With multiple sets of data from different directions, triangulation will allow for gradual buildup of the relative positions of the three targets (Figure 3). The range profiles are swept in the cross-range direction to form bands of constant range from the radar, which represent the possible locations of the target scatterers. These bands are then superimposed and the crossing points are used to determine the scattering center locations. The success of such a scheme hinges fundamentally on the ability to correlate the various constant range bands. Otherwise, the intersection of the swept lines will be erroneous, resulting in image artifacts.

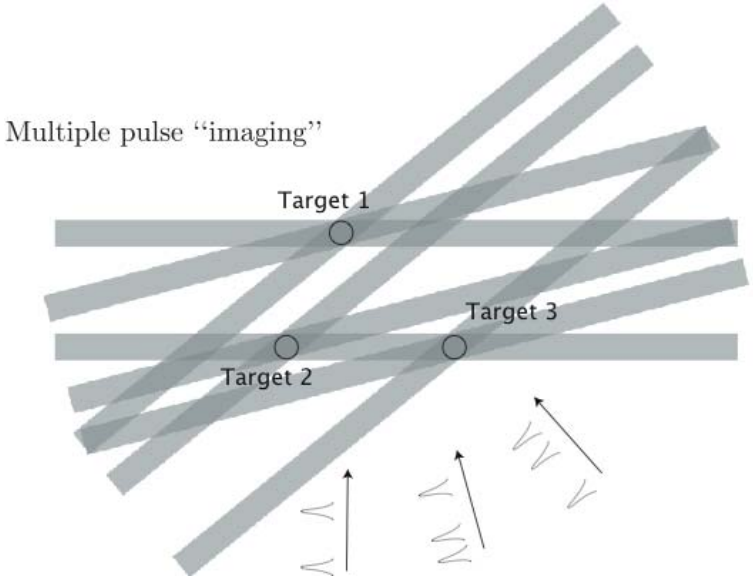

Figure 3. Cross-range information obtained from range profiles [19].

The signal due to a moving target is a time-delayed, Doppler-shifted version of the transmitted signal. The measured echo signal from a single point-like moving target can be expressed as

$$s_{rec}(t) = \rho s_{inc}(t-\tau)e^{-i\upsilon(t-\tau)} + n(t) \tag{2.14}$$

With two unknown parameters to estimate, namely the delay τ and the Doppler shift υ, a single matched filter will no longer suffice. A set of matched filters, one for every possible Doppler shift, will have to be applied

$$\eta(\tau,\upsilon) = \int_{-\infty}^{\infty} h_{\upsilon}(t-t')s_{rec}(t')dt' = \rho\int_{-\infty}^{\infty} h_{\upsilon}(t-t')s_{inc}(t'-\tau)e^{-i\upsilon(t'-\tau)}dt' \ + \text{ noise term}$$

To estimate τ and υ, find their values where $|\eta|$ takes on its maximum. For a distribution of non-interacting moving targets, the output from the filter bank is

$$\begin{aligned}
\eta(\tau,\upsilon) &= \int_{-\infty}^{\infty} s_{inc}^{*}(t'-\tau)e^{-i\upsilon(t'-\tau)}s_{rec}(t')dt' \\
&= \int_{-\infty}^{\infty} s_{inc}^{*}(t'-\tau)e^{-i\upsilon(t'-\tau)}\iint_{-\infty}^{\infty}\rho(\tau',\upsilon')s_{inc}(t'-\tau')e^{-i\upsilon'(t'-\tau')}d\tau'd\upsilon'dt' \\
&= \iiint_{-\infty}^{\infty} s_{inc}^{*}(t'-\tau)e^{-i\upsilon(t'-\tau)}s_{inc}(t'-\tau')e^{-i\upsilon'(t'-\tau')}dt'\rho(\tau',\upsilon')d\tau'd\upsilon' \\
&= \iiint_{-\infty}^{\infty} s_{inc}^{*}(t''+\tau'-\tau)e^{-i\upsilon(t''+\tau'-\tau)}s_{inc}(t'')e^{-i\upsilon'(t'')}dt''\rho(\tau',\upsilon')d\tau'd\upsilon' \\
&= \iint_{-\infty}^{\infty} \chi(\tau-\tau',\upsilon-\upsilon')e^{-i\upsilon'(\tau-\tau')}\rho(\tau',\upsilon')d\tau'd\upsilon'
\end{aligned} \tag{2.15}$$

where

$$\chi(\tau,\upsilon) = \int_{-\infty}^{\infty} s_{inc}^{*}(t''+\tau)e^{-i\upsilon(t'')}s(t'')dt'' = \int_{-\infty}^{\infty} s_{inc}^{*}(t'+\tau)s_{inc}(t')e^{-i\upsilon t'}dt' \tag{2.16}$$

is the *radar ambiguity function*. Similar to the one-dimensional case, the ambiguity function can be interpreted as an imaging point-spread function for range-Doppler imaging. Analysis of the ambiguity function determines the fidelity of the range-Doppler imaging process, and consequently the accuracy of target range and velocity estimation.

1. Range-Doppler Spatial Image

With estimates for range and range-rate from radar returns, this information can be interpreted to form spatial images. The following treatment illustrates this, provided the relative motion between the antenna and the target is known. Consider a simplified two-dimensional (2D) geometry between the radar and target as shown in (Figure 4). The target is assumed to have translational and rotational motion only in the two-dimensional plane relative to a stationary radar platform.

Consider a rotating target [18]. For simplification, assume that any overall translational motion is removed.

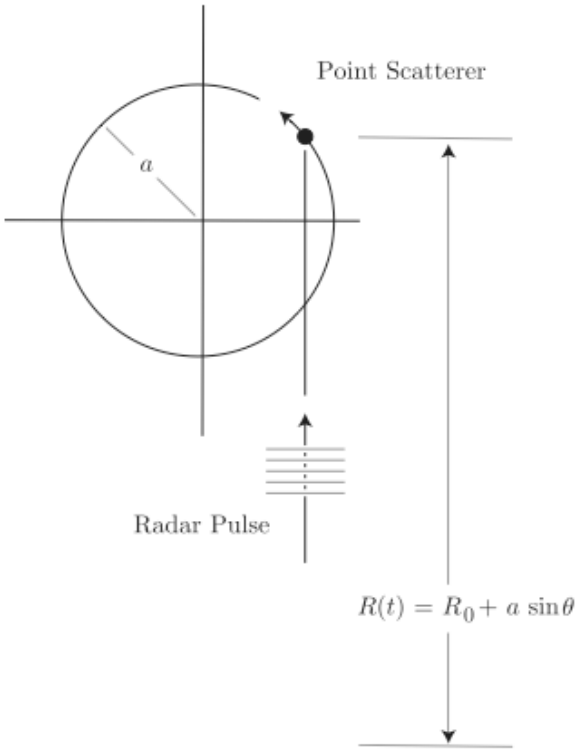

Figure 4. The geometry for locating a point target known to be rotating [18].

Consider a point target rotating counter-clockwise in a geometry in which the antenna is in the plane of rotation (Figure 4). The coordinate origin coincides with the center of rotation; and the center of rotation is a large distance R_0 from the radar antenna. The large range approximation means that the incident wave is approximately a plane

wave, consequently, all horizontal points are (approximately) at the same range. If the target is positioned at $(x, y) = a(\cos\theta, \sin\theta)$, then its range is

$$R = R_0 + y = R_0 + a\sin\theta \tag{2.17}$$

If its angular velocity is $\dot{\theta} = d\theta / dt$, then its velocity vector is $a\dot{\theta}(-\sin\theta, \cos\theta)$, its tangential speed is $|\upsilon| = a\dot{\theta}$, and the down range ($y$) component of the velocity is $\dot{R} = |\upsilon|\cos\theta = a\dot{\theta}\cos\theta$. However, since $x = a\cos\theta$, this down-range velocity can be written $\dot{R} = x\dot{\theta}$, where x is the cross-range component of the position. Note that for $x > 0$, the down-range velocity is negative, whereas for $x < 0$, it is positive.

This means that since a radar system can measure range $(R_0 + y)$ and range-rate $(\dot{R} = x\dot{\theta})$, it can determine the (x, y) location of the point in space (provided $\dot{\theta}$ is known). In particular, the radar measures the time delay $\tau = 2R / c$ and the Doppler shift

$$\upsilon_D = -\frac{2\dot{R}}{c}\upsilon_0 = -\frac{2x\dot{\theta}}{c}\upsilon_0$$

which means that the coordinates of the point are given by

$$(x, y) = \left(-\frac{\upsilon_D}{\upsilon_0}\frac{c}{2\dot{\theta}},\ \frac{c\tau}{2} - R_0\right) \tag{2.18}$$

This shows how the range-rate radar measurements can be used to estimate Doppler and cross-range information. Further, the simplification introduced highlights to the difficulties in practical implementation of the radar scattering model. Estimates of the scattered field requires any variations in range $\ddot{R}$ to be estimable. While it is reasonable to assume (in the one-dimensional imaging methods) $\ddot{R}$ as constant over the data set, the two-dimensional imaging schemes invariably will not. $\ddot{R}$ will generally vary due to the target (translational) motion that occurs during measurements made while the target rotates. The effect of failing to correctly account for this translational motion will be the introduction of phase errors into these data, and a source of image corruption.

F. RADAR IMAGING – AN INVERSE PROBLEM

A discussion of imaging theory will not be complete without addressing the inverse nature of the imaging problem and its associated issues. As the thesis is focused primarily on developing and analyzing the point spread function rather than imaging, the intent of this section is to highlight the key characteristics of such inverse problems – issues pertaining to practical measurement systems and how information is typically extracted from measurements to obtain the best estimates of the target object.

The radar can be well-approximated by a linear, shift-invariant system. This is an important characteristic, as it states that the object function $f(x)$ at each point x has a corresponding output image $m(x)$. Further, the system will measure objects the same no matter when they start (or, equivalently, where they are located). Radar imaging will not be meaningful if the delayed version of the target looks different. A general formulation of the imaging problem can be achieved by considering an imaging system represented by the functional operator ("kernel") κ that describes how the measurement system works

$$m = \kappa f \tag{2.19}$$

The *direct problem* in radar imaging refers to the mapping from the target to the quantities that can be measured by the radar. Consequently, the *inverse problem* is concerned with 'reproducing' the original target from given data and knowledge of the direct problem (in the case of radar imaging, it will be radar measurements and knowledge of the scattering model).

1. Well-Posed and Ill-Posed Problems

One of the issues for inverse problems is their ill-posed nature. An ill-posed problem is one whose solution is not unique and/or does not exist for any data and/or does not depend continuously on the data. In the case of a band-limited system, the solution of the inverse problem is not unique. This is because the imaging system does not transmit information about the target at frequencies outside the band of the measuring system.

Consider discretized measurement systems in which the measurements are collected at specific points, and so Equation (2.19) can be written in matrix form. And the basic goal of getting a good estimate $\bar{f}$ from the measurements *m* can be notionally represented as

$$\bar{f} = \kappa^{-1} m \tag{2.20}$$

It can be observed that κ, which represents the measurement system, imposes certain properties on the measurement system. In general, the matrix κ is $N \times M$ ($M > N$) as the object function is infinitely dimensional and will not be confined to the limitations of the measurement system. Consequently, Equation (2.20) has more unknowns than there are linearly independent equations and so the system cannot have a unique solution.

Since the object space (M-dimensional) is typically larger than the measurement space (N-dimensional), there exists what is known as the nullspace which consists of all vectors $f - \kappa f$ or, physically, all the things that *cannot be measured*. Nullspace accounts for measurement artifacts and is determined by the kernel κ.

The accepted approach for solving inverse problems which are ill-posed is to search for approximate solutions satisfying additional constraints based on the physics of the problem [22]. This set of approximate solutions corresponding to the same data function is the set of objects with images close to the measured one and is expressed in what are known as the normal equations

$$\kappa^T \kappa \bar{f} = \kappa^T m \tag{2.21}$$

2. Data Reconstruction – Regularization

Equation (2.21) specifies the set of conditions that must be satisfied by the least-squares solution $\bar{f}$ which can be rewritten as

$$\bar{f} = (\kappa^T \kappa)^{-1} \kappa^T m \tag{2.22}$$

Recall that the measured data suffers from finite dimension and noise contamination. These are problems since $(\kappa^T \kappa)$ is poorly conditioned and the effect of noise is

magnified (i.e. errors increase) as the dimensionality of the problem gets larger. Two techniques will be highlighted here, namely the singular value decomposition (SVD) and Tikhonov regularization, to mitigate the effects of noise when estimating $\bar{f}$.

From linear algebra methods, the matrix $(\kappa^T\kappa)^{-1}\kappa^T$ can be expressed in terms of its SVD [19]:

$$(\kappa^T\kappa)^{-1}\kappa^T = UDV^T \tag{2.23}$$

where the matrices *U*, *V* contain the eigenvectors of $(\kappa^T\kappa)$, and *D* will have diagonal elements of the form $1/\sqrt{\lambda_i}$ (where λ_i are the corresponding, non-zero eigenvalues). A consequence of the kernel κ being bounded is that the eigenvalues necessarily form a sequence that gets arbitrarily close to zero as the number of measurements increase. The diagonal elements of *D* get large when the higher dimensional data are used, and if the data are contaminated by noise, from Equations (2.22 and 2.23) that noise will also be multiplied by a large value. Hence, one simple approach to mitigate the noise effect is to truncate the SVD representation when λ_i falls below some chosen threshold value. The corresponding diagonal element is set to zero and this method is known as the *truncation filter*.

Tikhonov regularization modifies $(\kappa^T\kappa)^{-1}\kappa^T$ to a better conditioned form by adding a fixed scalar α to the original normal equations. Equation (2.22) can then be rewritten in the form

$$\bar{f} = (\kappa^T\kappa + \alpha I)^{-1}\kappa^T m \tag{2.24}$$

When $\alpha = 0$, the original normal equations are returned, so it can be expected that small values of α will not change the system description too much.

After introducing α, the diagonal elements of *D* in Equation (2.23) become

$$D_{ii} = \frac{\sqrt{\lambda_i}}{\lambda_i + \alpha} \tag{2.25}$$

When $\lambda_i \gg \alpha$, $D_{ii} \approx 1/\sqrt{\lambda_i}$ (as before). When $\lambda_i = \alpha$, however, $D_{ii} \approx \sqrt{\lambda_i}/\alpha$ and will not become arbitrarily large. Consequently, the noise problem is controlled.

THIS PAGE INTENTIONALLY LEFT BLANK

III. IMAGING DATA MODEL

This chapter develops an approach to imaging moving objects from scattered waves. Many of the ideas and concepts introduced in the preceding chapter will be extended to the three-dimensional case in order to develop the imaging model.

A. INTEGRAL EQUATION APPROACH TO SCATTERING

We have seen in the preceding chapter that for the one-dimensional scattering problem from a moving plate, the signal that returns to the radar is a time-delayed and frequency-shifted version of the transmitted signal. This is also the case for three-dimensional scattering from a moving, point-like target. A point target is the traditional model used for developing imaging analysis and will also be used for the thesis. The representation of a target as points is appropriate because for high-frequency waveforms scattered from smooth conducting surfaces, the net scattering effects from the surface is equivalent to the contribution from the entire series of points known as specular points [19].

Applying traditional electromagnetic approaches to scattering will typically involve solving a differential wave equation and imposition of appropriate boundary conditions at the surface of the scatterer. In practice, this process is difficult to implement for there is no coordinate system that can represent the boundary conditions for complex targets we encounter in practical scattering applications.

Hence, it is convenient to reformulate the scattering problem. It turns out that there exists an *equivalent integral equation* for every differential equation, and this integral equation can *intrinsically incorporate any boundary conditions in the solution*.

We take the scattering body to be located in free space and describable by an index of refraction $n(x)$. Consider a monochromatic wave, with harmonic time dependence (any signal can be built from these individual frequency component via superposition). The reduced wave equation for the field (Helmholtz equation) is

$$\nabla^2\Psi(x) + k^2 n^2(x)\Psi(x) = 0 \tag{3.1}$$

where k is the wave number in free space (note that $n(x) \neq 1$ on the scatterer). Splitting the field Ψ into the *incident field* Ψ_{inc} representing the incoming wave, and the *scattered field* Ψ_{scatt} and simplifying, Equation (3.1) yields

$$\begin{aligned} \nabla^2\Psi_{scatt}(x) + k^2\Psi_{scatt}(x) &= k^2(1-n^2(x))\left(\Psi_{inc}(x) + \Psi_{scatt}(x)\right) \\ &\equiv \rho(x)\left(\Psi_{inc}(x) + \Psi_{scatt}(x)\right) \end{aligned} \tag{3.2}$$

where the scattering density $\rho(x) = k^2\left(1-n^2(x)\right)$ is a source factor completely determined by the index of refraction of the scatterer *and is zero outside of the scatterer*.

A solution to Equation (3.2) can be obtained based on the application of *Green functions*, and we can write the solution as

$$\Psi_{scatt}(x) = \iiint_D G_k(x',x)\rho(x')\left(\Psi_{inc}(x') + \Psi_{scatt}(x')\right)d^3x' \tag{3.3}$$

This is a *Lippmann-Schwinger* equation. It can be observed that the problem of solving equation (1.1) has been reduced to finding the Green function $G_k(x',x)$ *in free space* (k denotes a specific frequency). The scattered field is also written as an integral over the *scatterer* D since $\rho(x) = 0$ otherwise, and hence automatically satisfies the required boundary conditions for a known target.

It is appropriate to make several additional observations with respect to the *Lippmann-Schwinger* equation:

(1) There are generally many functions that can serve as Green functions $G_k(x',x)$ *in free space*. While there are no bounding surfaces (other than those defined by the scattering object), we are interested in $G_k(x',x)$ that obey the Sommerfeld radiation condition $\lim_{r\to\infty} G_k(x',x) \propto \frac{1}{r}$

(2) The *inverse* scattering problem – i.e. that of determining ρ given Ψ_{inc} and Ψ_{scatt}, can also be approached using the *Lippmann-Schwinger* equation as a model for Ψ_{scatt}.

B. LINEARIZED DATA MODEL (TIME-VARYING SYSTEMS)

Enforcing the Born ("weak scatterer") approximation, where the object distribution (points) is not self-interacting, multiple scattering events are treated to be negligible in comparison with the primary scattering events. The resulting linearized (approximate) data model is

$$\Psi_{scatt}(x) = \iiint_D G_k(x',x)\rho(x')\Psi_{inc}(x')d^3x' \tag{3.4}$$

This solution is one for the Helmholtz equation. For time-varying systems, the time-dependent wave equation and the time-domain Green function will have to be incorporated within the model

$$G_k(x',x) \to g(x',x;t',t) = \frac{\delta(t-t'-|x'-x|/c)}{4\pi|x'-x|} \tag{3.5}$$

For a signal $s_y(t)$ transmitted from position *y* at starting time $-T_y$, the incident field at *x* is

$$\psi_{inc}(x,t) = -\frac{s_y(t+T_y-|x-y|/c)}{4\pi|x-y|} \tag{3.6}$$

and so the scattered field $\psi_{scatt}(y,z,t)$ at time *t* and position *z* obeys (Born approximation) is

$$\psi_{scatt}(y,z,t) = \iint \frac{\delta(t-t'-|z-x'|/c)}{4\pi|z-x'|}\frac{\ddot{s}_y(t'+T_y-|x'-y|/c)}{4\pi|x'-y|}\rho(x')d^3x'dt' \tag{3.7}$$

where $\ddot{s}_y$ denotes the second time derivative of $s_y(t)$ and enters as a consequence of the second time derivative in the wave equation.

C. REFLECTIVITY FUNCTION FOR MOVING TARGETS

The reflectivity function $\rho(x)$ or scattering density first introduced in Equation (3.2) is completely specified by the target scatterer. It is a scale factor of the received signal strength and an important characteristic of radar imaging. For a moving target, a time-varying reflectivity function $\rho(x,t)$ will be used. For an imaging scene containing multiple moving targets (or scatterers), the scattering model can be modified as follows: Let $\rho_v(x-vt)d^3xd^3v$ be the scatterers in the volume element d^3xd^3v of phase space centered at position *x* and velocity *v*. Choose T_y to be such that the scattering density $\rho_v = \rho_v(x)$ describes those targets moving with velocity *v* at time *t=0* (i.e., the transmitting antenna is activated at time $t=-T_y$). The spatial scatterer density centered at time *t* and position *x* is

$$\rho(x) = \int \rho_v(x-vt)d^3v \tag{3.8}$$

and the scattered field obeys

$$\begin{aligned}\psi_{scatt}(y,z,t) = \iiint & \frac{\delta(t-t'-|z-x'|/c)}{4\pi|z-x'|} \\ & \times \frac{\&_y(t'+T_y-|x'-y|/c)}{4\pi|x'-y|}\rho_v(x'-vt')d^3vd^3x'dt'\end{aligned} \tag{3.9}$$

Making the change of variables $x' \to x = x'-vt'$ (i.e., change to a frame of reference in which the scatterer ρ_v is fixed) to obtain

$$\begin{aligned}\psi_{scatt}(y,z,t) = \iiint & \frac{\delta(t-t'-|x+vt'-z|/c)}{4\pi|x+vt'-z|} \\ & \times \frac{\&_y(t'+T_y-|x+vt'-y|/c)}{4\pi|x+vt'-y|}\rho_v(x)d^3vd^3xdt'\end{aligned} \tag{3.10}$$

The physical interpretation is that the wave that emanates from *y* at time $-T_y$ encounters a target at time t'. This target, during the interval $[0,t']$, has moved from *x* to $x+vt'$.

The wave scatters with strength $\rho_v(x)$ and then propagates from position $x+vt'$ to *z*, arriving at time *t*.

Simplifying the notation, and writing

$$\boldsymbol{R}_{x,z}(t) = x + vt - z, \qquad R = |\,\boldsymbol{R}\,|, \qquad \hat{\boldsymbol{R}} = \boldsymbol{R} / R$$

then

$$\begin{aligned}\psi_{scatt}(y,z,t) = \iiint \frac{\delta(t - t' - R_{x,z}(t')/c)}{4\pi R_{x,z}(t')} \\ \times \frac{\ddot{\delta}(t' + T_y - R_{x,y}(t')/c)}{4\pi R_{x,y}(t')} \rho_v(x) d^3v d^3x dt'\end{aligned} \tag{3.11}$$

The variable *t'* in the argument of the delta function appears in several terms making it difficult to carry out the integral over *t'*. To address this, let $t' = \bar{t}_{x,\upsilon}(t)$ denote the implicit solution of

$$t - t' - R_{x,z}(t')/c = 0, \qquad \text{i.e.,} \quad t - \bar{t}_{x,v}(t) - R_{x,z}(\bar{t}_{x,v}(t))/c = 0$$

Then, performing the integration over t' yields

$$\psi_{scatt}(y,z,t) = \iint \frac{\ddot{\delta}\left(\bar{t}_{x,v}(t) + T_y - R_{x,y}(\bar{t}_{x,v}(t))/c\right)}{(4\pi)^2 R_{x,z}(\bar{t}_{x,v}(t)) R_{x,y}(\bar{t}_{x,v}(t))} \rho_v(x) d^3v d^3x$$

Substituting $\bar{t}_{x,v}(t) = t - R_{x,z}(\bar{t}_{x,v}(t))/c$ for the first occurrence of $\bar{t}_{x,v}(t)$ in this last equation allows for a more symmetric version

$$\psi_{scatt}(y,z,t) = \iint \frac{\ddot{\delta}\left(t + T_y - R_{x,z}(\bar{t}_{x,v}(t))/c - R_{x,y}(\bar{t}_{x,v}(t))/c\right)}{(4\pi)^2 R_{x,z}(\bar{t}_{x,v}(t)) R_{x,y}(\bar{t}_{x,v}(t))} \rho_v(x) d^3v d^3x \tag{3.12}$$

D. FURTHER SIMPLIFYING APPROXIMATIONS

Equation (3.12) applies to very general circumstances. It applies to rapidly moving targets (where the start-stop approximation is not valid), and is appropriate for arbitrary transmitted waveforms.

However, Equation (3.12) is also a manifestation of retarded-time problems, which are invariably complex. The complications arise as a consequence of the definition of retarded time $\bar{t}_{x,v}(t)$, which is obtained implicitly from the relation $\bar{t}_{x,v}(t) = t - R_{x,z}(\bar{t}_{x,v}(t))/c$. A more tractable result can be obtained when the scatterers are known to be moving in such a way that $R_{x,z}(t)$ can be expanded in a Taylor series around *t=0* and approximated by retaining only the terms linear in *t* - i.e., when the scatterer is "slow moving".

1. Slow-Mover Approximation

Assume that $(|v|t)$ and $(|v|^2 t^2 \times \omega_{\max}/c)$ are much less than $|x-z|$ and $|x-y|$ (where $\omega_{\max}$ denotes the maximum angular frequency of the transmitted signal s_y). In this case,

$$R_{x,z}(t) = |z-(x-vt)| = R_{x,z}(0) + \ddot{\boldsymbol{R}}_{x,z}(0)\boldsymbol{g}\boldsymbol{y}t + \ldots$$

where $\boldsymbol{R}_{x,z}(0) = \boldsymbol{x} - \boldsymbol{z}$, $R_{x,z}(0) = |\boldsymbol{R}_{x,z}(0)|$, and $\ddot{\boldsymbol{R}}_{x,z}(0) = \boldsymbol{R}_{x,z}(0)/R_{x,z}(0)$. Substituting this result into the definition of retarded time yields

$$\begin{aligned}\bar{t}_{x,v}(t) &\approx t - \left(R_{x,z}(0) + \ddot{\boldsymbol{R}}_{x,z}(0)\boldsymbol{g}\boldsymbol{y}\bar{t}_{x,\upsilon}(t)\right)/c \\ &\approx \frac{t - R_{x,z}(0)/c}{1 + \ddot{\boldsymbol{R}}_{x,z}(0)\boldsymbol{g}\boldsymbol{y}/c}\end{aligned}$$

Inserting this approximation into the result for $\psi_{scatt}(y,z,t)$ yields

$$\psi_{scatt}(y,z,t) = \iint \frac{\&\&\left(\alpha_{x,v}\left[t - R_{x,z}(0)/c\right] - R_{x,y}(0)/c + T_y\right)}{(4\pi)^2 R_{x,z}(0) R_{x,y}(0)} \rho_v(x)\, d^3v\, d^3x \qquad (3.13)$$

where

$$\alpha_{x,v} \equiv \frac{1 - \ddot{\boldsymbol{R}}_{x,y}(0)\boldsymbol{g}\boldsymbol{y}/c}{1 + \ddot{\boldsymbol{R}}_{x,z}(0)\boldsymbol{g}\boldsymbol{y}/c} \qquad (3.14)$$

is the Doppler scale factor. Similar to the traditional Doppler shift, it is closely related to the velocity component in target-transmitter direction.

2. Slow-Mover and Narrow-Band Approximation

Typical systems are narrow-band for which the transmitted signal is of the form

$$s_y(t) = \psi_y(t)e^{-i\omega_y t}$$

where $\psi_y(t)$ is slowly varying (as a function of t) in comparison with $e^{-i\omega_y t}$ (where ω_y is the carrier frequency for the transmitter at position y). In this case, the time derivatives of s_y are dominated by the $e^{-i\omega_y t}$ factor, and $\ddot{s}_y(t) \approx -\omega_y^2 \psi_y(t)e^{-i\omega_y t}$. Moreover, since $\psi_y(t)$ is slowly varying, further approximations can be made

$$\psi_y(\alpha_{x,v}t)e^{-i\omega_y \alpha_{x,v} t} \approx \psi_y(t)e^{-i\omega_y \alpha_{x,v} t} \tag{3.15}$$

Equation (3.13), under the slow-mover and narrow-band then becomes

$$\begin{aligned}\psi_{scatt}(y,z,t) = -\iint & \frac{\omega_y^2 e^{i\varphi_{x,v}} e^{-i\omega_y \alpha_{x,v} t}}{(4\pi)^2 R_{x,z}(0) R_{x,y}(0)} \\ & \times \psi_y\left(t + T_y - (R_{x,z}(0) + R_{x,y}(0))/c\right) o_v(x) d^3v d^3x\end{aligned} \tag{3.16}$$

where

$$\varphi_{x,v} \equiv \omega_y^2 \left[R_{x,y}(0) - cT_y + \alpha_{x,v} R_{x,z}(0) \right] / c \tag{3.17}$$

3. Slow-Mover, Narrow-Band and Far-Field Approximation

When the transmitter-to-target and target-to-receiver distances are large in comparison with the scene dimensions, then $|x + vt|$ and $|x + vt|^2 \times \omega_{\max} / c$ can be assumed to be much less than either $|z|$ or $|y|$. And the expansion

$$R_{x,z}(t) = |z - (x - vt)| = |z| - \hat{z} \cdot (x + vt) + \ldots$$

can be applied (and similarly for $R_{x,y}(t)$). Substituting the expansions into previous approximations (Equation (3.16)) then yields

$$\psi_{scatt}(y,z,t) \approx \frac{-\omega_y^2}{(4\pi)^2 |z||y|} \iint e^{i\varphi_{x,v}} e^{-i\omega_y \alpha_{x,v} t} \times s_y\left(t + T_y - (|z| - \hat{z}\cdot\mathbf{x} + |y| - \hat{y}\cdot\mathbf{x})/c\right) \rho_v(x) d^3v d^3x \tag{3.18}$$

where now

$$\varphi_{x,v} \equiv \omega_y \left[|y| - \hat{y}\cdot\mathbf{x} - cT_y + \alpha_v (|z| - \hat{z}\cdot\mathbf{x}) \right] / c \tag{3.19}$$

Note that in Equation (3.16), the expansions for $R_{x,z}(t)$, $R_{x,y}(t)$ are used differently. In the amplitude factor the approximation $R_{x,z}(t) = |z - (x + vt)| \approx |z|$ holds since $|z| \gg |\hat{z}\cdot(x + vt)|$; in the phase factor, however, the product $(\hat{z}\cdot\mathbf{x} \times \omega_{\max}/c)$ can still be a large fraction of 2π, and must be retained. In addition, the signal envelope s_y can still vary significantly over $|z| - \hat{z}\cdot\mathbf{x}$ despite being slowly varying, hence the first order term is retained.

The Doppler scale factor also reduces to

$$\alpha_v \approx \frac{1 - \hat{y}\cdot\mathbf{v}/c}{1 + \hat{z}\cdot\mathbf{v}/c} \approx 1 - (\hat{y} + \hat{z})\cdot\mathbf{v}/c \tag{3.20}$$

where the binomial expansion is used since $|\mathbf{v}|/c \ll 1$. The quantity $\omega_y \times \beta_v$ is the Doppler shift (where $\beta_v \equiv -(\hat{y} + \hat{z})\cdot\mathbf{v}/c$) and is observed to be dependent on the "bistatic" vector $(\hat{y} + \hat{z})$.

Inserting $T_y = |y|/c$ and setting $k_y \equiv \omega_y / c$

$$\varphi_{x,v} \equiv k_y |\mathbf{z}| - k_y (\hat{y} + \hat{z})\cdot\left[\mathbf{x} + (\hat{z}\cdot(\mathbf{z} - \mathbf{x}))\mathbf{v}/c \right] \tag{3.21}$$

E. IMAGING VIA A FILTERED ADJOINT

In developing the correlation receiver, it was observed that the "fit" between two (complex-valued) functions is given by the cross correlation. For correlation reception, the correlation integral seeks out the component of received signal that "matches" the time-delayed, frequency-shifted version of the transmitted signal. Large values of the correlation integral indicate a strong resemblance, while small values indicate weak resemblance. The values of the time-delay and Doppler shift parameters, which maximized the correlation integral, were also the parameters most likely to represent the target.

Using the same notion, imaging can be achieved by determining the position and velocity parameters that represent the best "fit" to the measured data. These will also be the parameters that localize the position and velocity of the unknown scatterers in phase space (position-velocity) space. Cross correlation in the time domain, is multiplication in the Fourier transform domain (*Fourier correlation theorem*) – hence the association with filtering since filters are multiplication operators in the Fourier transform domain.

The model developed for $\psi_{scatt}(y,z,t)$ depends on the position of the scatterer $\boldsymbol{x} = (x_1, x_2, x_3)$ and its velocity $\boldsymbol{v} = (v_1, v_2, v_3)$. Using this form for $\psi_{scatt}(y,z,t)$ to build a six-parameter scattering model based on the arbitrary position $\boldsymbol{p} = (p_1, p_2, p_3)$ and arbitrary velocity $\boldsymbol{u} = (u_1, u_2, u_3)$, the objective will be to determine the values of $\boldsymbol{p}$ and $\boldsymbol{u}$ that maximize the cross correlation between the arbitrary model and the measured data.

In terms of the Doppler shift, the scattered field (from known scatterers $\rho_v(x)$ with positions *x* and velocities *v*) is

$$\psi_{scatt}(y,z,t) \approx \frac{-\omega_y^2 e^{-i\omega_y(t-|z|/c)}}{(4\pi)^2 |z||y|} \iint \exp\left\{-ik_y(\ddot{y}+\ddot{z})[x - v(t - z(z-x)/c)]\right\} \times \delta\left(t - (|z| - (\ddot{y}+\ddot{z})(x)/c\right)\rho_v(x)d^3v d^3x$$

The effect of data shifted in time is an image that is translated in range. Since this has no bearing on the imaging process, the scattered field result can be simplified by substituting $t' = t - |z|/c$ which yields

$$\psi_{scatt}(y,z,t') \approx \frac{-\omega_y^2 e^{-i\omega_y t'}}{(4\pi)^2 |z||y|} \iint \exp\left\{-ik_y(\hat{y}+\hat{z})[x - v(t'+\hat{z}\cdot x/c)]\right\} \times s_y\left(t'+(\hat{y}+\hat{z})\cdot x/c\right)\rho_v(x)d^3v\,d^3x$$

Ignoring the intensity prefactor, a parametric model representing the field from an unknown point source is

$$\psi(y,z,t') = -e^{-i\omega_y t'} \exp\left\{-ik_y(\hat{y}+\hat{z})[p - u(t'+\hat{z}\cdot p/c)]\right\} \times s_y\left(t'+(\hat{y}+\hat{z})\cdot p/c\right) \tag{3.22}$$

And the image is created as follows: For each *p* and *u*, determine the function

$$I(p,u) = \iiint \psi_{scatt}(y,z,t')\psi^*(y,z,t')dt'\,d^m y\,d^n z \tag{3.23}$$

where *m*, *n* depends on the configuration of the transmitter(s)/receiver(s), and the integrals are over all values of t', *y* and *z* for which measured data is available.

$$I(p,u) = \iiint \psi_{scatt}(y,z,t')\psi^*(y,z,t')Q(\omega,t',p,u,y,z)dt'\,d^m y\,d^n z$$

$$I(p,u) = -\iiint Q(\omega,t',p,u,y,z)e^{i\omega_y t'}e^{ik_y(\hat{y}+\hat{z})[p-u(t'+\hat{z}\cdot p/c)]} \times s_y\left(t'+(\hat{y}+\hat{z})\cdot p/c\right)\psi_{scatt}(y,z,t')dt'\,d^m y\,d^n z$$

IV. IMAGING POINT SPREAD FUNCTION

This chapter begins by looking at the radar ambiguity function, and the relationship between the transmitted waveform, and the accuracy with which target range and velocity can be estimated. The imaging point-spread function (PSF) is also derived based on the imaging scheme developed in Chapter III.

A. RADAR AMBIGUITY FUNCTION

For a stationary target, the output of the correlation receiver is the cross correlation between (1) the received signal plus noise and (2) the transmitted signal. In many radar applications, however, the target is moving so that its echo signal has a Doppler frequency shift. The output is hence a cross correlation between the received signal and the Doppler-shifted transmitted signal.

The nature of the correlation receiver output as a function of both time and Doppler frequency is important for understanding the properties of a radar waveform, in particular its effect on measurement *accuracy*, target *resolution*, and *ambiguities* in range and radial velocity. These aspects of the correlation receiver output will be examined in turn.

When the received echo signal is large compared to noise, the output of the correlation receiver may be written as the following (see Equations (2.15) and (2.16))

$$\eta(\upsilon,\tau) = \iint_{-\infty}^{\infty} \rho(\upsilon',\tau')\chi(\upsilon-\upsilon',\tau-\tau')e^{i\frac{1}{2}(\upsilon+\upsilon')(\tau-\tau')}d\tau' d\upsilon'$$

where $\chi(\upsilon-\upsilon',\tau-\tau')$ is the radar ambiguity function. The problem of radar imaging is concerned with estimating the location and strength of the point scatterers that are assumed to make up the target. Consequently, understanding χ is essential as the end state involves 'inverting' the radar data model. By definition, we have

$$\chi(\upsilon-\upsilon',\tau-\tau') = \int_{-\infty}^{\infty} s_{inc}\left(t'-\frac{1}{2}(\tau-\tau')\right)s_{inc}^{*}\left(t'+\frac{1}{2}(\tau-\tau')\right)e^{i(\upsilon-\upsilon')t'}dt' \qquad (4.1)$$

1. Basic Properties

For simplicity, the origin is chosen to be the true target time-delay and frequency-shift. This assumption will be carried throughout the rest of the discussion. Some key properties that follow from Equation (4.1) [Refs. 14, 18 and 19] are listed

$$\textbf{Signal energy :} \quad \left|\chi(\upsilon,\tau)\right| \le \left|\chi(0,0)\right| \tag{4.2}$$

$$\textbf{Ambiguity volume :} \quad \iint_{-\infty}^{\infty} \left|\chi(\upsilon,\tau)\right|^2 d\tau d\upsilon = 1 \qquad (\textit{normalized signal}) \tag{4.3}$$

$$\textbf{Symmetry :} \quad \left|\chi(-\upsilon,-\tau)\right| = \left|\chi(\upsilon,\tau)\right| \tag{4.4}$$

$$\textbf{Frequency - domain :} \quad \chi(\upsilon,\tau) = \frac{1}{2\pi}\int_{-\infty}^{\infty} s_{inc}(\omega - \frac{1}{2}\upsilon) s_{inc}^{*}(\omega + \frac{1}{2}\upsilon) e^{-i\omega\tau} d\omega \tag{4.5}$$

Equation (4.2) states that the maximum value of the ambiguity function occurs at the origin (true target time-delay and frequency-shift). Equation (4.3) asserts that the total volume under the ambiguity surface is a constant. This gives rise to a *radar uncertainty principle*: choosing a signal $s(t)$ so that the ambiguity surface will be narrow in one dimension will cause it to be correspondingly wide in the other dimension. In the case of range-Doppler imaging, a waveform with good range resolution has poor Doppler resolution and vice versa.

2. Range Resolution

Equation (4.5) presents an intuitive look at range resolution. Consider a fixed target $(\upsilon = 0)$ and rewrite Equation (4.5) as

$$|\chi(0,\tau)| = \frac{1}{2\pi}\left|\int_{-\infty}^{\infty} |s_{inc}(\omega)|^2 e^{-i\omega\tau} d\omega\right| \tag{4.6}$$

Recognize the form of Equation (4.6) as the inverse Fourier transform (of the transmitted power spectral density). Then, in order for $|\chi(0,\tau)|$ to have high resolution in τ measurements (ideally a delta function), the power spectral density has to be identically

one; such a signal will have infinite energy or broadly supported in the Fourier domain. Hence, it is clear that better range resolution is obtained when the signal bandwidth is broad.

A more rigorous study for estimation errors (in the presence of Gaussian noise) is developed in [1] by examining the behavior of the ambiguity function in the neighborhood of its main peak. This study shows that estimation error of υ and τ is described by an ellipse, and that time-domain resolution is inversely proportional to frequency-domain bandwidth. Hence, bandwidth is inherently important to problems in radar target imaging. A further interesting result makes use of the definition of bandwidth in terms of the second moments (probabilistic variance) of the power spectrum to yield (for a narrow-band signal $s(t) = a(t)e^{i\Phi(t)}$). We can write

$$\beta^2 = \frac{1}{2}\int_{-\infty}^{\infty}\left|\frac{da(t')}{dt'}\right|^2 dt' + \frac{1}{2}\int_{-\infty}^{\infty}\left(\frac{d\Phi(t')}{dt'}\right)^2 |a(t')|^2\, dt' - \omega_0^2 \tag{4.7}$$

where β represents bandwidth. The useful relationship illustrates a nonlinear $\Phi(t)$ (phase modulation) will increase the bandwidth in comparison with signals that are modulated in amplitude only. This is the basis for pulse compression (see Chapter V), a technique of practical importance since it allows for the creation of fine range-resolution waveforms that are also of long duration (with sufficient energy on target).

3. Doppler Resolution

To study Doppler resolution, consider a target whose range is known. Thus, setting $\tau = 0$ in Equation (4.1) yields

$$|\chi(\upsilon,0)| = \left|\int_{-\infty}^{\infty} |s_{inc}(t')|^2 e^{i\upsilon t'} dt'\right| \tag{4.8}$$

It is evident that better Doppler resolution is obtained from a long duration signal. This is in stark contrast to range resolution requirements. In addition, the Doppler resolution is determined only by the amplitude modulation of the signal and not by the phase.

B. IMAGE ANALYSIS

From Chapter III, an explicit form for the image is

$$I(p,u) = -\iiint Q(\omega,t',p,u,y,z)e^{i\omega_y t'}e^{ik_y(\ddot{y}+\ddot{z})\left[p-u(t'+\ddot{z}p/c)\right]} \times s_y\left(t'+(\ddot{y}+\ddot{z})p/c\right)\psi_{scatt}(y,z,t')dt'd^m y d^n z \tag{4.9}$$

To examine the performance of the imaging scheme, the ideal (expected) data are inserted back into the image equation. Substituting for $\psi_{scatt}(y,z,t')$ yields

$$I(p,u) = \iiint\iint \frac{\omega_y^2 Q(\omega,t',p,u,y,z)}{(4\pi)^2 |z||y|}\rho_v(x) \times \exp\left\{ik_y(\ddot{y}+\ddot{z})\left[p-x-(u-v)t'-u(\ddot{z}p)/c+v(\ddot{z}x)/c\right]\right\} \times s_y\left(t'+(\ddot{y}+\ddot{z})p/c\right)s_y\left(t'+(\ddot{y}+\ddot{z})x/c\right)d^3v d^3x dt' d^m y d^n z \tag{4.10}$$

The distances $|z|$ and $|y|$ are scaling amplitude factors and not essential for imaging purposes. Thus, choose

$$Q(\omega,t',p,u,y,z) = \frac{(4\pi)^2|z||y|}{\omega_y^2}J(p,u,y,z) \tag{4.11}$$

where $J(p,u,y,z)$ depends on the geometry and is chosen to compensate for a Jacobian that results from the integral of the variable *t'*

$$I(p,u) = \iiint\iint s_y\left(t'+(\ddot{y}+\ddot{z})p/c\right)s_y\left(t'+(\ddot{y}+\ddot{z})x/c\right)e^{-ik_y(y+z)(u-v)t'} \times \exp\left\{ik_y(\ddot{y}+\ddot{z})\left[p-x-u(\ddot{z}p)/c+v(\ddot{z}x)/c\right]\right\} \times J(p,u,y,z)\rho_v(x)dt'd^3v d^3x d^m y d^n z \tag{4.12}$$

which is

$$I(p,u) = \iint K(p,u,y,z)\rho_v(x)d^3v d^3x \tag{4.13}$$

where

$$K(p,u,y,z) = \iint \exp\left\{-ik_y(\ddot{y}+\ddot{z})[u(\ddot{z}-p) - v(\ddot{z}-x)]/c\right\}$$
$$\times \int s_y^*\left(t' + (\ddot{y}+\ddot{z})\cdot p/c\right) s_y\left(t' + (\ddot{y}+\ddot{z})\cdot x/c\right) e^{-ik_y(\ddot{y}+\ddot{z})(u-v)t'} dt' \qquad (4.14)$$
$$\times J(p,u,y,z) d^m y d^n z$$

is the point-spread function describing the behavior of the imaging system. Apply the change of variables $t = t' + \frac{1}{2}(\ddot{y}+\ddot{z})\cdot(p+x)/c$ and set $\tau \equiv (\ddot{y}+\ddot{z})\cdot(p-x)/c$ to obtain

$$K(p,u,y,z) = \iint \exp\left\{-ik_y(\ddot{y}+\ddot{z})[u(\ddot{z}-p) - v(\ddot{z}-x)]/c\right\}$$
$$\times \exp\left\{ik_y(\ddot{y}+\ddot{z})\left[(p-x) + \frac{1}{2}(u-v)(\ddot{y}+\ddot{z})\cdot(p+x)\right]/c\right\} \qquad (4.15)$$
$$\times \left[\int_{-\infty}^{\infty} s_y^*\left(t+\frac{1}{2}\tau\right) s_y\left(t-\frac{1}{2}\tau\right) e^{-ik_y(\ddot{y}+\ddot{z})\cdot(u-v)t} dt\right] J(p,u,y,z) d^m y d^n z$$

The integral in square brackets is the radar ambiguity function

$$\chi(\upsilon,\tau) = \int_{-\infty}^{\infty} s_y^*\left(t+\frac{1}{2}\tau\right) s_y\left(t-\frac{1}{2}\tau\right) e^{-i\upsilon t} dt$$

χ is determined by the transmitted signal and $|\chi|$ attains its maximum value at $p = x$, $u = v$ (for general configurations of transmitter/receiver). So the imaging PSF can be written as

$$K(p,u,y,z) = \iint \exp\left\{-ik_y(\ddot{y}+\ddot{z})[u(\ddot{z}-p) - v(\ddot{z}-x)]/c\right\}$$
$$\times \exp\left\{ik_y(\ddot{y}+\ddot{z})\left[(p-x) + \frac{1}{2}(u-v)(\ddot{y}+\ddot{z})\cdot(p+x)\right]/c\right\} \qquad (4.16)$$
$$\times \chi\left(k_y(\ddot{y}+\ddot{z})\cdot(u-v), (\ddot{y}+\ddot{z})\cdot(p-x)/c\right) J(p,u,y,z) d^m y d^n z$$

THIS PAGE INTENTIONALLY LEFT BLANK

V. PULSE COMPRESSION

Detection of signals in noise and resolving capability are both fundamental to radar imaging. As discussed in Chapter II and IV, the use of correlation reception and a transmitted waveform with non-linear phase modulation provides means to enhance performance in detection and resolution. Pulse compression is a technique that fuses these concepts and involves transmitting long coded pulses, together with signal processing methods such as correlation reception. This is of practical importance since it allows for the creation of fine range-resolution waveforms that are also of long duration (this increases radiation energy directed on target without relying solely on boosting radar transmitted power). This chapter gives a physical interpretation of pulse compression and looks at a specific phase-coded signal known as the *chirp*.

A. REVISITING CORRELATION RECEPTION

Recall in Chapter II, the output of the correlation receiver is a correlation integral between the received signal and a time-delayed, Doppler-shifted version of the transmitted signal. It is illustrative to explain the phenomenon of pulse compression with a graphical example. Using the simple one-dimensional imaging case in Equation (2.12), the correlation receiver output can be written as

$$\eta(t) = \int_{-\infty}^{\infty} s^*(t') s_{rec}(t'+t)\,dt' \tag{5.4}$$

which is a *correlation* between *s* and s_{rec}. If $s = s_{rec}$ (reflectivity function is 1), Equation (5.4) is called an *autocorrelation*. In Figure 5. the signal at the top represents the transmitted waveform. The lower graphs represent the received signal for different shifts, according to Equation (5.4). When a signal shifted by *t* is multiplied by the waveform at the top and the product is integrated over *t'*, the resulting number is plotted at position *t* on the graph to the right.

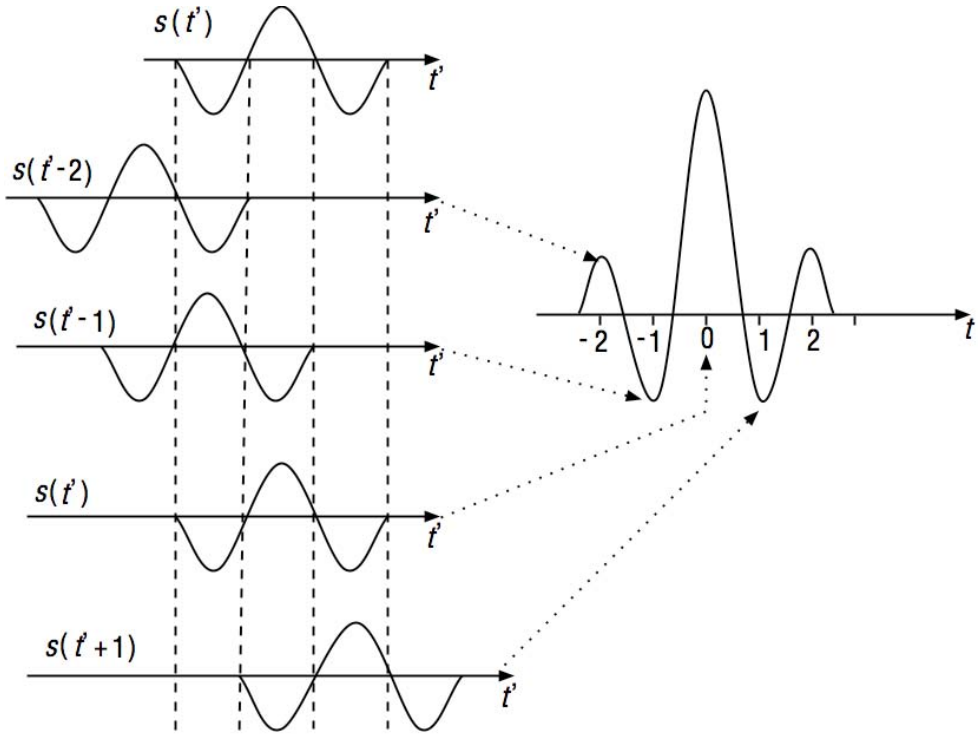

Figure 5. Phenomenon of pulse compression where the energy is concentrated at a single delay time [18].

Figure 5 shows that, although the output signal has a longer time duration than the original signal *s*, its energy is more concentrated at a single delay time. It is a consequence of the Cauchy-Schwarz inequality that the highest peak occurs when the signals are not shifted relative to each other. The smaller peaks, called sidelobes, are undesirable and an open problem is to design pulses whose autocorrelations have the lowest and fewest sidelobes. An issue that has direct bearing on signal detection as the received signal is expected to "look" like a time-delayed, Doppler-shifted version of itself.

B. PHASE CODING – CHIRPS

A radar system makes the most efficient use of power when it transmits a constant-amplitude waveform. Consequently, most radar waveforms are designed with variations only in the phase of the signal. The most important and most commonly-used radar waveform is the *chirp*. A chirp is a constant-amplitude signal whose instantaneous

frequency varies linearly with time; chirps are therefore also called *Linearly Frequency Modulated* (LFM) waveforms. Linear variation of the instantaneous frequency implies that $d\phi / dt = \omega_{\min} + \gamma t$. The coefficient γ is called the (angular) *chirp rate*. A chirp is thus of the form

$$s(t) = e^{i(\omega_{\min} t + \frac{1}{2}\gamma t^2)} u_{[0,T]}(t) \tag{5.5}$$

where $u_{[0,T]}(t)$ is 1 in the interval [0, T] and 0 otherwise.

A chirp with positive chirp slope is called an upchirp; one with a negative chirp slope is a downchirp. The instantaneous (angular) frequency of the chirp varies from $\omega_{\min}$ to $\omega_{\max} = \omega_{\min} + \gamma t$, with a center frequency of $\omega_0 = \omega_{\min} + \gamma t / 2$. Thus the instantaneous frequency of the chirp varies over the interval $\left[\omega_0 - T\gamma / 2, \omega_0 + T\gamma / 2\right]$. The power spectrum of a chirp is roughly constant over the frequency band $\left[\omega_0 - T\gamma / 2, \omega_0 + T\gamma / 2\right]$, thus the angular frequency bandwidth $T\gamma$ can be estimated by looking at the range of instantaneous frequencies (see Figure 6).

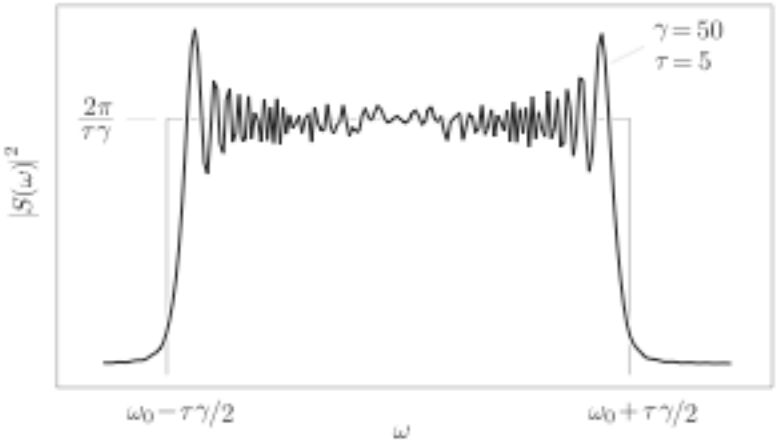

Figure 6. Spectrum for a chirp pulse of length τ [1].

Chirps are very commonly used in radar imaging. Pulse compression for chirps has the following intuitive interpretation: When the pulse is transmitted, different parts of

the pulse are coded with different instantaneous frequencies. In the pulse compression process, the different frequencies are delayed by different amounts of time, so that all the energy emerges at the same time [18].

C. AMBIGUITY FUNCTION FOR COMMON WAVEFORMS

From the preceding discussion, the "ideal" ambiguity function will typically consist of a single peak of infinitesimal thickness at the origin and be zero everywhere else. It will closely approximate an impulse function, and have no ambiguities in range or Doppler frequency. The infinitesimal thickness at the origin will permit the time delay and/or frequency to be determined simultaneously to as high a degree of accuracy as desired. Such a highly desirable ambiguity function, however, is not theoretically allowed. The properties of the ambiguity function implicitly mandate that trade-offs exist between the measured dimensions.

In practice, other than the trade-offs in dimension resolution, waveforms also generally have significant response outside the narrow region in the near vicinity of the origin, i.e. there are many possible ambiguous (blind) range and Doppler. Ambiguities are a consequence of discontinuous waveforms, such as in a pulse train. The resolution for single rectangular pulse, single chirp and coherent pulse trains will be discussed next.

1. Resolution for a Single Rectangular Pulse

Time domain impulses have infinite bandwidth, hence they are idealized signals. More realistic waveforms can be modeled, for example, as

$$s_{inc}(t) = \begin{cases} 1 & \text{if } 0 < t \le T, \\ 0 & \text{otherwise.} \end{cases} \tag{5.6}$$

for which $s_{inc}(t - 1/2\tau)s^{*}_{inc}(t + 1/2\tau)$ is non-zero in the interval $t \in (|\tau|/2,\ T - |\tau|/2)$.

The ambiguity function is then

$$\chi(\upsilon,\tau) = \int_{-\infty}^{\infty} s_{inc}(t'-\frac{1}{2}\tau)s_{inc}^{*}(t'+\frac{1}{2}\tau)e^{i\upsilon t'}dt' = \int_{|\tau|/2}^{T-|\tau|/2} e^{i\upsilon t'}dt'$$
$$= \frac{1}{i\upsilon}e^{i\upsilon(T/2)}\left[e^{i\upsilon(T/2-|\tau|/2)} - e^{-i\upsilon(T/2-|\tau|/2)}\right] \qquad (5.7)$$
$$= (T-|\tau|)e^{i\upsilon T/2}\mathrm{sinc}\left[\frac{1}{2}\upsilon(T-|\tau|)\right]$$

For $\upsilon = 0$, then the delay resolution (by the peak-to-first-null measure) as observed from the ambiguity surface $|\chi(0,\tau)|^2$, is $\Delta\tau = T$ (zero-crossing at $\tau = T$), which corresponds to a range resolution of $\Delta R = cT/2$. For $\tau = 0$, the ambiguity surface $|\chi(\upsilon,0)|^2$ yields $\Delta\upsilon = 1/T$ since the first zero of the *sinc* function occurs when its argument is π. The Doppler shift is related to down-range relative velocity by $\upsilon_D = -2v\upsilon_0/c$ (see Equation (2.4)), and the corresponding velocity resolution is $\Delta v = \lambda_0/2T$.

2. Resolution for a Single Chirp

This is another example of a ridge type ambiguity function produced by linearly frequency modulating a rectangular pulse over a bandwidth β. The pulse width T is large compared to $1/\beta$. The frequency modulation increases the spectral bandwidth of the pulse so that βT ? 1. Since the pulse width T and the bandwidth β can be chosen independent of one another, the time-delay and frequency accuracies are independent of the other.

The *chirp* signal is one whose frequency changes linearly with time

$$s_{inc}(t) = \begin{cases} \exp\left(-i\frac{1}{2}\gamma t^2\right) & \text{if } 0 < t \le T, \\ 0 & \text{otherwise.} \end{cases} \qquad (5.8)$$

The constant γ is known as the *chirp rate*. The ambiguity function is then

$$\begin{aligned}\chi(\upsilon,\tau) &= \int_{-\infty}^{\infty} s_{inc}(t'-\frac{1}{2}\tau)s_{inc}^{*}(t'+\frac{1}{2}\tau)e^{i\upsilon t'}dt' = \int_{|\tau|/2}^{T-|\tau|/2} e^{i(\upsilon+\gamma\tau)t'}dt' \\ &= \frac{1}{i(\upsilon+\gamma\tau)}e^{i(\upsilon+\gamma\tau)T/2}\left[e^{i(\upsilon+\gamma\tau)(T/2-|\tau|/2)} - e^{-i(\upsilon+\gamma\tau)(T/2-|\tau|/2)}\right] \\ &= (T-|\tau|)e^{i(\upsilon+\gamma\tau)T/2}\text{sinc}\left[\frac{1}{2}(\upsilon+\gamma\tau)(T-|\tau|)\right]\end{aligned} \tag{5.9}$$

Observe that a chirp leads to an ambiguity function that is a *sinc*-function in both the time and frequency domain. It is instructive to examine this property again by looking at the signal resolution.

For $\tau = 0$, similar result of $\Delta\upsilon = 1/T$ is obtained as in the case of the rectangular pulse. This is because the amplitude modulation is identical in both cases. Consequently, Doppler resolution is the same. However, with phase modulation, it is expected that the delay resolution (hence range resolution) will be enhanced.

For $\upsilon = 0$, when $\tau > 0$ the first null occurs when $\pi = (T-\tau)\gamma\tau/2$. Reference [19] shows that the expression $\pi = (T-\tau)\gamma\tau/2$ has a quadratic equation form with a solution $\Delta\tau = 2\pi/\gamma T$, which corresponds to a range resolution of $\Delta R = c/\beta$ where $\beta = 2\pi\gamma T$ is the bandwidth (in Hertz). For $\tau = 0$, $\Delta\upsilon = |\chi(\upsilon,0)|^2 = 1/T$ since the first zero of the *sinc* function occurs when its argument is π. The Doppler shift is related to down-range relative velocity by $\upsilon_D = -2v\upsilon_0/c$ (see Equation (2.4)), and the corresponding velocity resolution $\Delta v = \lambda_0/2T$.

The pulse compression ratio is defined as the product of pulse spectral bandwidth β and the uncompressed pulsewidth *T*. Comparing the range resolution between the single rectangular pulse and single chirp,

$$\frac{\Delta R_{\text{rectangular}}}{\Delta R_{\text{chirp}}} = \frac{cT/2}{c/\beta} = \frac{\beta T}{2} \tag{5.10}$$

In other words, phase modulation improves the range resolution by a factor of one-half the time-bandwidth product.

3. Resolution for Coherent Pulse Trains

Following the analysis given in [18], a train of *N* identical pulses is considered:

$$s(t) = \frac{1}{\sqrt{N}} \sum_{n=0}^{N-1} u(t - nT_R) \tag{5.11}$$

where T_R is the pulse repetition interval, which might be on the order of 1ms. The reciprocal $1/T_R$ is called the pulse repetition frequency (PRF).

The ambiguity function for the pulse train is

$$\begin{aligned} \chi(\upsilon,\tau) &= \frac{1}{N} \sum_{n=0}^{N-1} \sum_{m=0}^{N-1} \int u^*(\tau + \tau' - mT_R) u(\tau' - nT_R) e^{i\upsilon\tau'} d\tau' \\ &= \frac{1}{N} \sum_{n=0}^{N-1} \sum_{m=0}^{N-1} \chi_u\left(\tau - (n-m)T_R, \upsilon\right) e^{i\upsilon nT_R} \end{aligned} \tag{5.12}$$

where χ_u denotes the ambiguity function for *u* and where we have used the substitution $t'' = \tau' - nT_R$. A lengthy calculation involving rearrangement of the order of summation and the summing of a geometric series results in

$$\chi(\upsilon,\tau) = \frac{1}{N} \sum_{p=-(N-1)}^{N-1} \chi_u(\tau - pT_R, \upsilon) e^{i\upsilon T_R (N-1-|p|)} \frac{\sin\left[\pi\upsilon T_R (N - |p|)\right]}{\sin(\pi\upsilon T_R)} \tag{5.13}$$

If the pulses *u* are sufficiently well-separated so their ambiguity functions χ_u do not overlap, then we take the absolute value of Equation (5.13) to obtain

$$|\chi(\upsilon,\tau)| = \frac{1}{N} \sum_{p=-(N-1)}^{N-1} |\chi_u(\tau - pT_R, \upsilon)| \left| \frac{\sin\left[\pi\upsilon T_R (N - |p|)\right]}{\sin(\pi\upsilon T_R)} \right| \tag{5.14}$$

Such an ambiguity function has a "bed of nails" appearance (see Figure 7), with peaks at $\tau = pT_R$, $p = -(N-1),-(N-2),...,0,1,...,(N-1)$ and υ such that $\pi\upsilon T_R N = (m+1/2)\pi$, $m = 0,1,2,...$

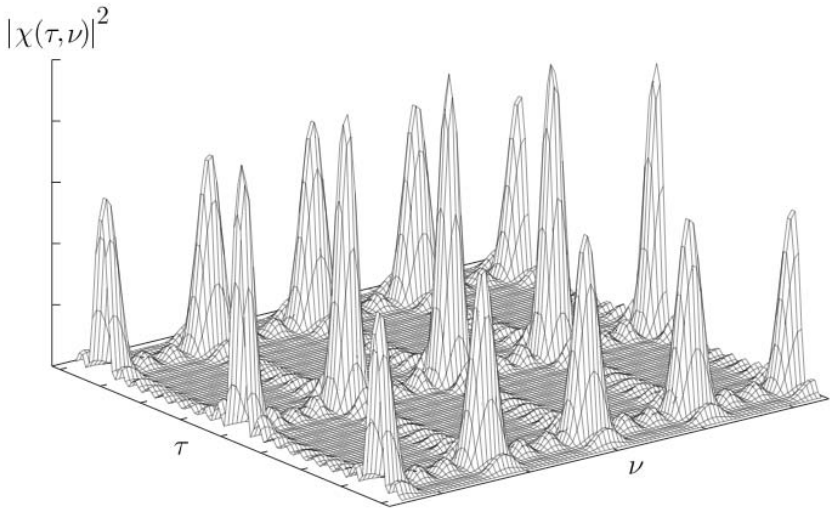

Figure 7. Ambiguity function for a train of pulses.

Following previous analysis, consider the $\upsilon = 0$ cut of the ambiguity surface to estimate the range resolution yields

$$|\chi(0,\tau)| = \frac{1}{N}\sum_{p=-(N-1)}^{N-1} |\chi_u(\tau - pT_R, 0)|(N - |p|) \tag{5.15}$$

where we have used the fact that $\lim_{x\to 0}[\sin bx]/\sin x = b$. We see that the range resolution of the main peak is the same as the range resolution of the individual pulse *u*, but that we now have range ambiguities due to the extraneous peaks at $\tau = pT_R$.

To estimate the Doppler resolution, consider the $\tau = 0$ cut of Equation (5.14) and for well-separated pulses, only the *p=0* term contributes

$$|\chi(\upsilon,0)| = \frac{1}{N}\sum_{p=-(N-1)}^{N-1} |\chi_u(0,\upsilon)|\left|\frac{\sin[\upsilon T_R N]}{\sin[\upsilon T_R]}\right| \tag{5.15}$$

Consider the numerator argument since it varies much faster. It shows that the Doppler resolution is $1/NT_R$, and hence, the Doppler resolution of the pulse train is higher than that of a single pulse.

The many ambiguities produced by a pulse train may appear to lead to a poor radar waveform. The time-delay measurement accuracy (determined by pulsewidth *T*) and the frequency accuracy (determined by the pulse repetition interval T_R) can be selected independently. If pulse repetition interval T_R is such that no radar echoes are expected with a time delay greater than T_R, and no Doppler-frequency shifts are expected greater than $1/T_R$, then the effective ambiguity function reduces to just a single spike at the origin whose dimensions are determined by *T* and T_R. In practice, ambiguities can also be resolved with different PRF, and many radars employ this type of waveform.

THIS PAGE INTENTIONALLY LEFT BLANK

VI. RESULTS AND CONCLUSION

Here, analysis of the imaging point-spread function (PSF) (Equation (4.16)) is carried out using Matlab. Equation (4.16) does not restrict the choice of the transmitted waveform nor the transmitter/receiver configuration. The goal here is to study the behavior of the PSF under different waveforms and transmitter/receiver configuration.

Figure 8 shows the transmitter/receiver geometries for the simulation performed. The receivers are denoted by "z1" to "z8" while the transmitter is denoted by "y1". For configurations of two to four receivers, the geometry as shown in Figure 8(a) is used, while Figure 8(b) shows the geometry for eight receivers.

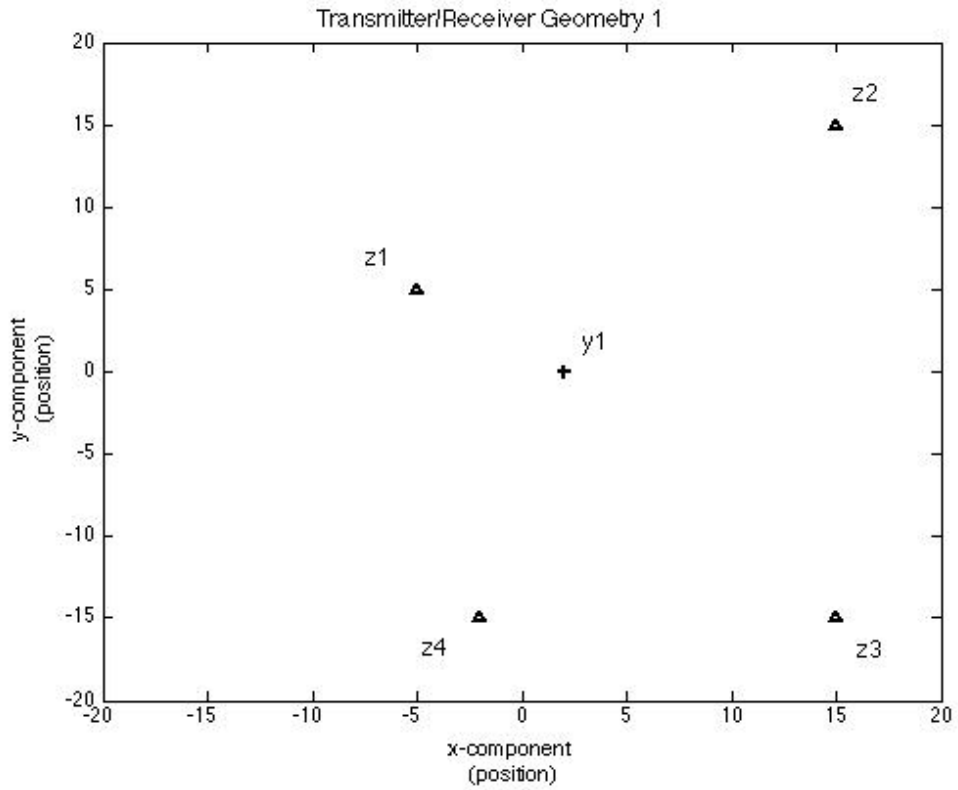

(a)

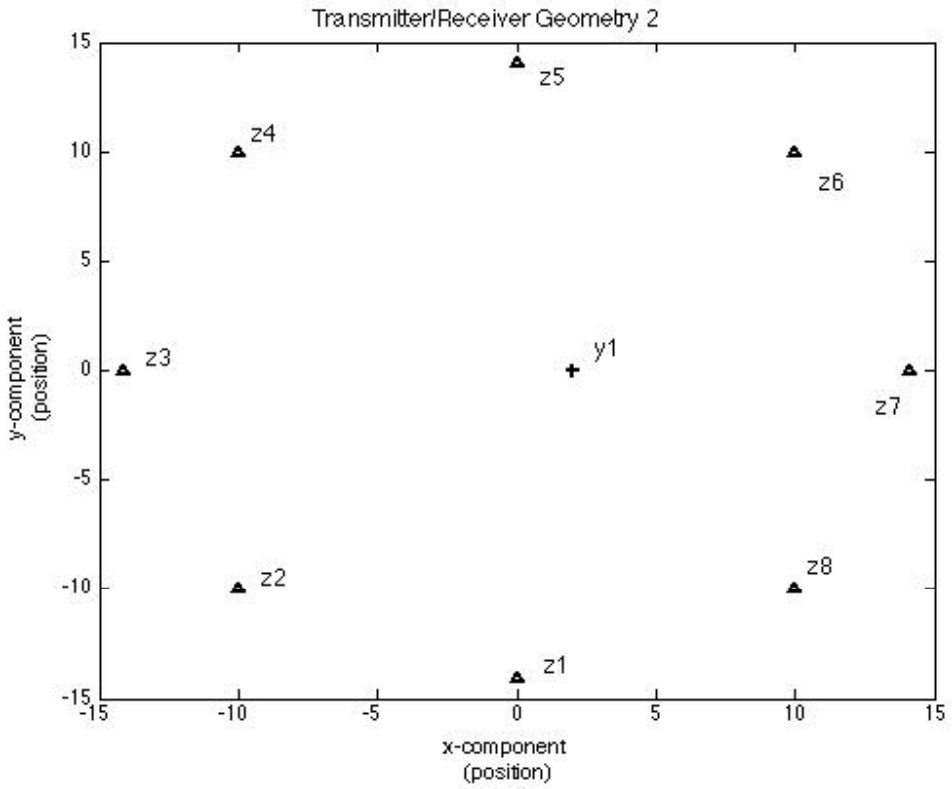

(b)

Figure 8. Transmitter/Receiver configuration for 2, 3, 4 and 8 receivers.

A. IMAGING PSF FOR SINGLE RECTANGULAR PULSE

The transmitted waveform is single rectangular pulse defined in Equation (5.6). Its associated ambiguity function (Equation (5.7)) is substituted into the imaging PSF, Equation (4.16) and implemented in Matlab. Equation (4.16) is capable of determining a three-dimensional distribution of positions in space and the corresponding three-dimensional velocities (i.e. a six-dimensional phase space image). However, to study the effects of transmitter/receiver geometry and translation in position/velocity on the imaging PSF, separate two-dimensional plots of the PSF in position and velocity space will suffice.

1. Localization of Point-Scatterer in Position Space

The point scatterer is located at position $(x_1, x_2) = (0,0)$. Two-dimensional plots of the imaging PSF in position space for two, three, four and eight receivers are given in Figures 9(a)-(d) respectively. Clearly, the point scatterers are localized in position space about the scatterer position (0,0). However, under the different geometries, the point scatterer is represented differently, with the 'two receivers' case resembling the least like a point. In Figure 9(a), the point scatterer appears longish and rectangular in shape. These distortions of the point scatterer are responsible for the image artifacts encountered during imaging. The extent of the PSF distortions will determine the level of artifacts produced. In Figure 9(d), the PSF appears as a blob and one will expect to see smudges in the resulting image. It can be observed that the geometry of the transmitters/receiver plays a role in shaping the PSF.

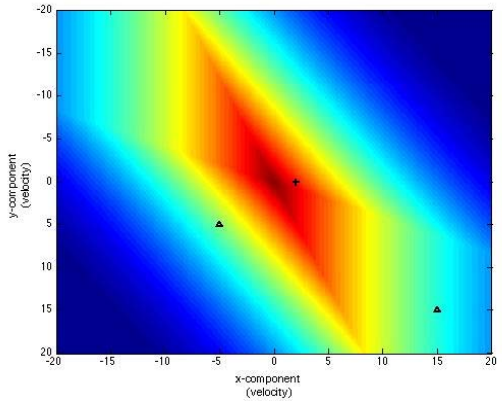

(a)

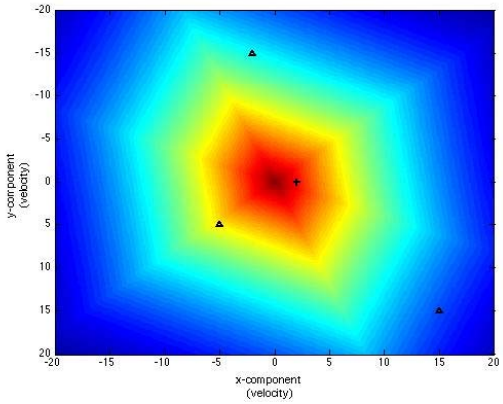

(b)

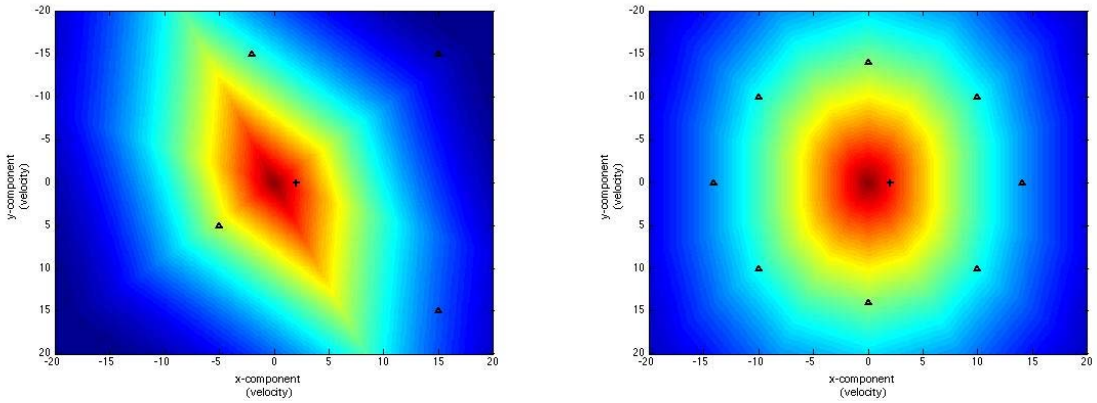

(c) (d)

Figure 9. 2-D Localization of point-scatterer in position space (for rectangular pulse).

Figure 10 shows the point-scatterer is relocated to position $(x_1, x_2) = (5,5)$. The resulting imaging PSF becomes localized now at the new position (5,5). The PSF retains its shape, and the characteristic of translation (in position) invariance for the PSF is necessary for a good imaging system.

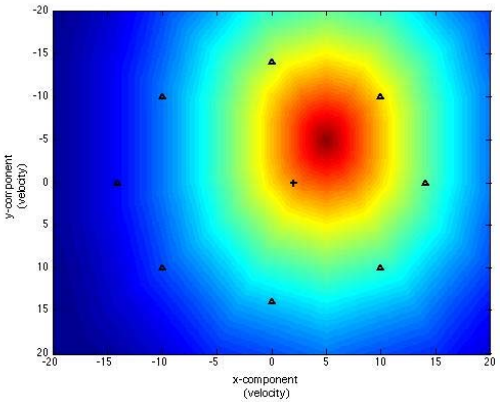

Figure 10. Position invariance of imaging PSF.

2. Localization of Point-Scatterer in Velocity Space

The point scatterer is located at velocity $(v_1, v_2) = (0,0)$. Two-dimensional plots of the imaging PSF in velocity space for two, three, four and eight receivers are given in

Figures 11(a)-(d) respectively. Clearly, the point scatterers are also localized in velocity space, and similar to the case in position space, the geometry of the transmitters/receiver plays a role in the shape of the PSF. The velocity resolution is visibly poorer.

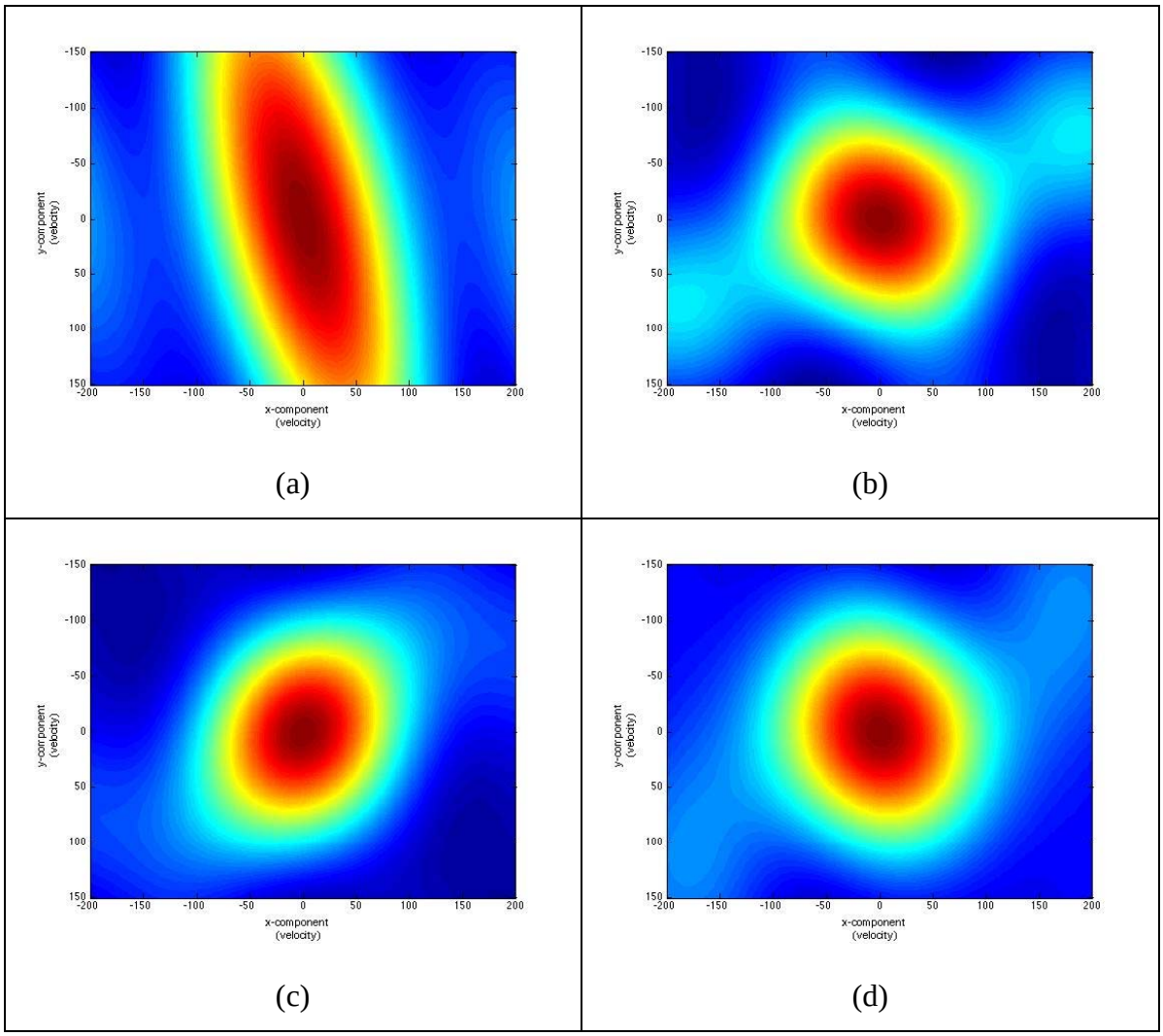

Figure 11. 2-D Localization of point-scatterer in velocity space (for rectangular pulse).

When the point-scatterer is moving with a new velocity of $(v_1, v_2) = (-35, -50)$, Figure 12 shows that the resulting imaging PSF becomes localized now at the new velocity $(-35, -50)$. The imaging PSF demonstrates similar translation invariance in the velocity space.

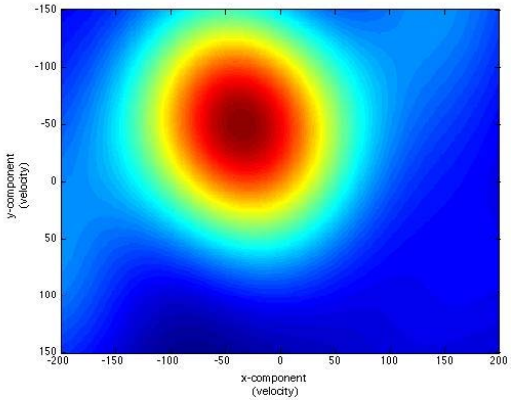

Figure 12. Velocity invariance of imaging PSF.

B. IMAGING PSF FOR SINGLE CHIRP

In Chapter V, it was shown that a chirp signal improves range resolution. The associated ambiguity function for a single chirp (Equation (5.9)) is substituted into the imaging PSF, Equation (4.16) and implemented in Matlab.

1. Localization of Point-Scatterer in Position Space

Again, the point scatterer is located at position $(x_1, x_2) = (0,0)$. Two-dimensional plots of the imaging PSF in position space for two, three, four and eight receivers are given in Figures 13(a)-(d) respectively. The PSF is visibly better localized as compared to transmitting a rectangular pulse.

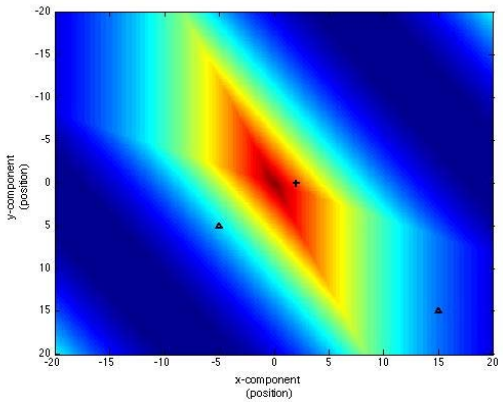

(a)

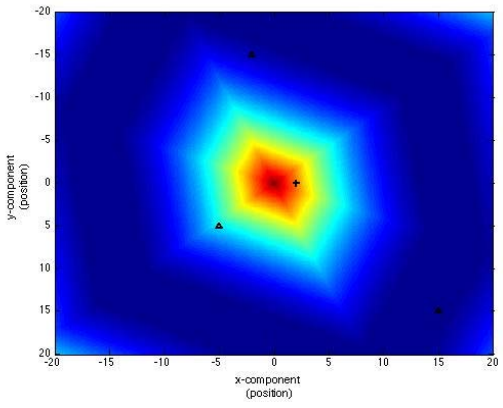

(b)

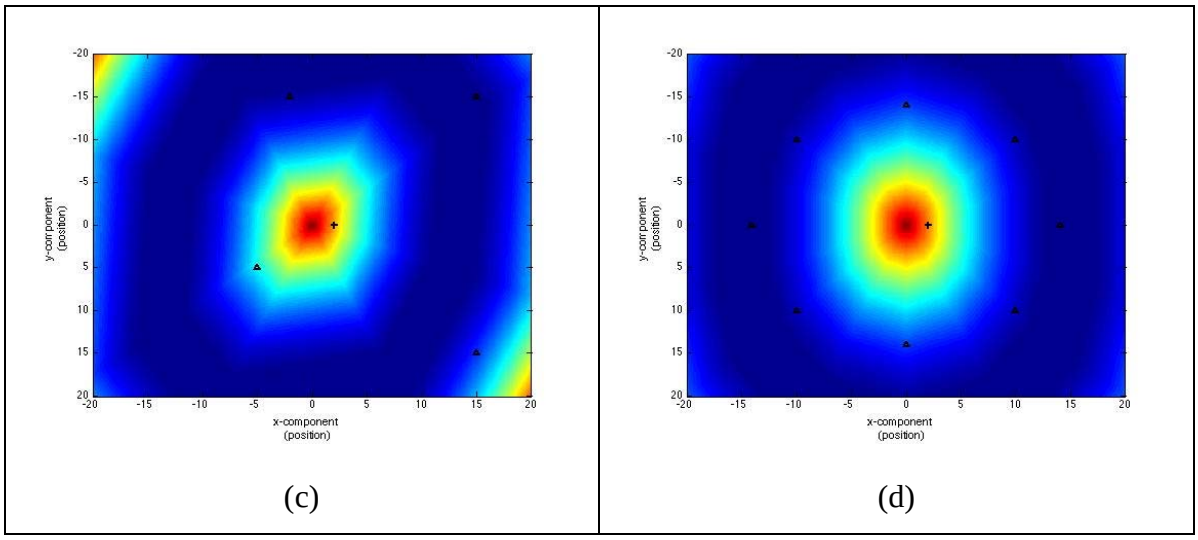

Figure 13. 2-D Localization of point-scatterer in position space (for chirp signal).

C. CONCLUSION

Image artifacts result when motion in the imaging scene is not addressed. In recent years, a number of attempts to develop imaging techniques that can handle moving objects have been proposed, however, all of these techniques rely on making the approximation that a target in motion is assumed to be momentarily stationary while it is being interrogated by a radar pulse. This thesis is a study of the new imaging approach developed by *Cheney*, *Borden* [2] that can accommodate target motion during the imaging process.

In this thesis, the subject of radar imaging from scattered waves is explored and applied to derive the corresponding imaging point-spread function for the new imaging approach. The simulation result (using Matlab) obtained showed that the imaging point-spread function is well behaved, specifically it localizes the target in phase space and is translation invariant. In addition, it is apparent that the geometry of the transmitters and receivers disposition affects the behavior of the point-spread function, and hence the imaging system.

This work represents the early stages of development of a full imaging algorithm applicable to moving targets in a multistatic environment. Follow-on work will include further simulation efforts. This thesis used single pulse radar waveforms and a single

transmitter, but in reality, fielded radar systems typically utilize pulse compression techniques and send out long, coded pulse trains. Neither need the multistatic radar system be restricted to one transmitter. In this case, the imaging point-spread function has to be adjusted to incorporate more realistic radar waveforms and optimize the transmitter/receiver geometries for implementing the imaging algorithm. These will be used to support the development of the eventual imaging algorithm. Finally, real world target data can then be applied to the developed imaging algorithm to assess its performance.

APPENDIX: MATLAB CODES

```
%%%%%%%%%%%%%%%%%
%  This program evaluates the Point Spread Function (PSF)
%  The program uses the approach, techniques on imaging from Professor
Borden, %  Brett

%  It is a six-parameter scattering model based on arbitrary position
%  p=(p_x,p_y,p_z) & velocity u=(u_x,u_y,u_z)
%%%%%%%%%%%%%%%%%

clear all

%%  Variables to be specified
x=(10^3)*[0;0;0];              % actual target
v=[0;0;0];                     % actual target velocity
y1=[2;0;0];                    % transmitter_1
z1=[-5;5;0];                   % receiver_1
z2=[15;15;0];                  % receiver_2
z3=[-2;-15;0];                 % receiver_3
z4=[-10;10;0];
z5=[0;14.1;0];
z6=[10;10;0];
z7=[14.1;0;0];
z8=[10;-10;0];
u=[0;0;0];
pulse=10^(-4);

%%  Parameters Defined
Y1=(1/sqrt(y1(1)^2+y1(2)^2+y1(3)^2)).*y1;
Z1=(1/sqrt(z1(1)^2+z1(2)^2+z1(3)^2)).*z1;
Z2=(1/sqrt(z2(1)^2+z2(2)^2+z2(3)^2)).*z2;
Z3=(1/sqrt(z3(1)^2+z3(2)^2+z3(3)^2)).*z3;
Z4=(1/sqrt(z4(1)^2+z4(2)^2+z4(3)^2)).*z4;
Z5=(1/sqrt(z5(1)^2+z5(2)^2+z5(3)^2)).*z5;
Z6=(1/sqrt(z6(1)^2+z6(2)^2+z6(3)^2)).*z6;
Z7=(1/sqrt(z7(1)^2+z7(2)^2+z7(3)^2)).*z7;
Z8=(1/sqrt(z8(1)^2+z8(2)^2+z8(3)^2)).*z8;
J=1;                           % Jacobian
c=3*10^8;
k_y=2*pi*(10^10)/c;            % wave vector @f=10 GHz

%%  PSF Range Defined
p_x_start=-20;
p_x_end=20;
p_y_start=-20;
p_y_end=20;
res_p=0.1;                     % resolution of p
p_x=p_x_start:res_p:p_x_end;  % define vector of x-axis values
p_y=p_y_start:res_p:p_y_end;  % define vector of y-axis values

%%  PSF Velocity Defined
u_x_start=-200;
u_x_end=200;
u_y_start=-150;
u_y_end=150;
res_u=1;
u_x=u_x_start:res_u:u_x_end;
u_y=u_y_start:res_u:u_y_end;
```

```
%%%%%%%%%%%%%%%%
Localization in Position-Space
%%%%%%%%%%%%%%%%

nx=length(p_x);               % length of x = columns in K
ny=length(p_y);               % length of y = rows in K
K=zeros(ny,nx);               % initialize K matrix
K1=zeros(ny,nx);
K2=zeros(ny,nx);
K3=zeros(nx,ny);
K4=zeros(nx,ny);
K5=zeros(nx,ny);
K6=zeros(nx,ny);
K7=zeros(nx,ny);
K8=zeros(nx,ny);

for m=1:ny
    for n=1:nx
        p=(10^3)*[p_x_start+((n-1)*res_p);p_y_end-((m-1)*res_p);0];

        % for receiver_1
        arg1_1=((Y1+Z1).')*((u*((Z1.')*p))-(v*((Z1.')*x)));
        phase1_1=exp(-i*k_y*arg1_1/c);
        arg2_1=((Y1+Z1).')*((p-x)+(0.5*(u-v)*(((Y1+Z1).')*(p+x))));
        phase2_1=exp(i*k_y*arg2_1/c);
        tau_1=1/c*(((Y1+Z1).')*(p-x));
        neu_1=k_y*(((Y1+Z1).')*(u-v));
        %rectangular pulse
        amb_1=pi*(pulse-abs(tau_1))*exp(-
i*0.5*neu_1*pulse)*sinc((0.5/pi)*(-neu_1)*(pulse-abs(tau_1)));
        K1(m,n)=phase1_1*phase2_1*amb_1*J;

        % for receiver_2
        arg1_2=((Y1+Z2).')*((u*((Z2.')*p))-(v*((Z2.')*x)));
        phase1_2=exp(-i*k_y*arg1_2/c);
        arg2_2=((Y1+Z1).')*((p-x)+(0.5*(u-v)*(((Y1+Z2).')*(p+x))));
        phase2_2=exp(i*k_y*arg2_2/c);
        tau_2=1/c*(((Y1+Z2).')*(p-x));
        neu_2=k_y*(((Y1+Z2).')*(u-v));
        amb_2=pi*(pulse-abs(tau_2))*exp(-
i*0.5*neu_2*pulse)*sinc((0.5/pi)*(-neu_2)*(pulse-abs(tau_2)));
        K2(m,n)=phase1_2*phase2_2*amb_2*J;

        % for receiver_3
        arg1_3=((Y1+Z3).')*((u*((Z3.')*p))-(v*((Z3.')*x)));
        phase1_3=exp(-i*k_y*arg1_3/c);
        arg2_3=((Y1+Z3).')*((p-x)+(0.5*(u-v)*(((Y1+Z3).')*(p+x))));
        phase2_3=exp(i*k_y*arg2_3/c);
        tau_3=1/c*(((Y1+Z3).')*(p-x));
        neu_3=k_y*(((Y1+Z3).')*(u-v));
        amb_3=pi*(pulse-abs(tau_3))*exp(-
i*0.5*neu_3*pulse)*sinc((0.5/pi)*(-neu_3)*(pulse-abs(tau_3)));
        K3(m,n)=phase1_3*phase2_3*amb_3*J;
        % for receiver_4
        arg1_4=((Y1+Z4).')*((u*((Z4.')*p))-(v*((Z4.')*x)));
        phase1_4=exp(-i*k_y*arg1_4/c);
        arg2_4=((Y1+Z4).')*((p-x)+(0.5*(u-v)*(((Y1+Z4).')*(p+x))));
        phase2_4=exp(i*k_y*arg2_4/c);
        tau_4=1/c*(((Y1+Z4).')*(p-x));
        neu_4=k_y*(((Y1+Z4).')*(u-v));
        amb_4=pi*(pulse-abs(tau_4))*exp(-
i*0.5*neu_4*pulse)*sinc((0.5/pi)*(-neu_4)*(pulse-abs(tau_4)));
        K4(m,n)=phase1_4*phase2_4*amb_4*J;
```

```
        % for receiver_5
        arg1_5=((Y1+Z5).')*((u*((Z5.')*p))-(v*((Z5.')*x)));
        phase1_5=exp(-i*k_y*arg1_5/c);
        arg2_5=((Y1+Z5).')*((p-x)+(0.5*(u-v)*(((Y1+Z5).')*(p+x))));
        phase2_5=exp(i*k_y*arg2_5/c);
        tau_5=1/c*(((Y1+Z5).')*(p-x));
        neu_5=k_y*(((Y1+Z5).')*(u-v));
        amb_5=pi*(pulse-abs(tau_5))*exp(-
i*0.5*neu_5*pulse)*sinc((0.5/pi)*(-neu_5)*(pulse-abs(tau_5)));
        K5(m,n)=phase1_5*phase2_5*amb_5*J;

        % for receiver_6
        arg1_6=((Y1+Z6).')*((u*((Z6.')*p))-(v*((Z6.')*x)));
        phase1_6=exp(-i*k_y*arg1_6/c);
        arg2_6=((Y1+Z6).')*((p-x)+(0.5*(u-v)*(((Y1+Z6).')*(p+x))));
        phase2_6=exp(i*k_y*arg2_6/c);
        tau_6=1/c*(((Y1+Z6).')*(p-x));
        neu_6=k_y*(((Y1+Z6).')*(u-v));
        amb_6=pi*(pulse-abs(tau_6))*exp(-
i*0.5*neu_6*pulse)*sinc((0.5/pi)*(-neu_6)*(pulse-abs(tau_6)));
        K6(m,n)=phase1_6*phase2_6*amb_6*J;

        % for receiver_7
        arg1_7=((Y1+Z7).')*((u*((Z7.')*p))-(v*((Z7.')*x)));
        phase1_7=exp(-i*k_y*arg1_7/c);
        arg2_7=((Y1+Z7).')*((p-x)+(0.5*(u-v)*(((Y1+Z7).')*(p+x))));
        phase2_7=exp(i*k_y*arg2_7/c);
        tau_7=1/c*(((Y1+Z7).')*(p-x));
        neu_7=k_y*(((Y1+Z7).')*(u-v));
        amb_7=pi*(pulse-abs(tau_7))*exp(-
i*0.5*neu_7*pulse)*sinc((0.5/pi)*(-neu_7)*(pulse-abs(tau_7)));
        K7(m,n)=phase1_7*phase2_7*amb_7*J;

        % for receiver_8
        arg1_8=((Y1+Z8).')*((u*((Z8.')*p))-(v*((Z8.')*x)));
        phase1_8=exp(-i*k_y*arg1_8/c);
        arg2_8=((Y1+Z8).')*((p-x)+(0.5*(u-v)*(((Y1+Z8).')*(p+x))));
        phase2_8=exp(i*k_y*arg2_8/c);
        tau_8=1/c*(((Y1+Z8).')*(p-x));
        neu_8=k_y*(((Y1+Z8).')*(u-v));
        amb_8=pi*(pulse-abs(tau_8))*exp(-
i*0.5*neu_8*pulse)*sinc((0.5/pi)*(-neu_8)*(pulse-abs(tau_8)));
        K8(m,n)=phase1_8*phase2_8*amb_8*J;

K(m,n)=(abs(K1(m,n)+K2(m,n)+K3(m,n)+K4(m,n)+K5(m,n)+K6(m,n)+K7(m,n)+K8(m
,n))).^2;

    end
end

%%%%%%%%%%%%%%%%
Localization in Velocity-Space
%%%%%%%%%%%%%%%%

nx=length(u_x);              % length of x = columns in K
ny=length(u_y);              % length of y = rows in K
K=zeros(ny,nx);
K1=zeros(ny,nx);
K2=zeros(ny,nx);
K3=zeros(ny,nx);
K4=zeros(ny,nx);
K5=zeros(ny,nx);
```

```
K6=zeros(ny,nx);
K7=zeros(ny,nx);
K8=zeros(ny,nx);

for m=1:ny
    for n=1:nx
        u=[u_x_start+((n-1)*res_u);u_y_end-((m-1)*res_u);0];

        % for receiver_1
        arg1_1=((Y1+Z1).')*((u*((Z1.')*p))-(v*((Z1.')*x)));
        phase1_1=exp(-i*k_y*arg1_1/c);
        arg2_1=((Y1+Z1).')*((p-x)+(0.5*(u-v)*(((Y1+Z1).')*(p+x))));
        phase2_1=exp(i*k_y*arg2_1/c);
        tau_1=1/c*(((Y1+Z1).')*(p-x));
        neu_1=k_y*(((Y1+Z1).')*(u-v));
        amb_1=pi*(pulse-abs(tau_1))*exp(-
i*0.5*neu_1*pulse)*sinc((0.5/pi)*(-neu_1)*(pulse-abs(tau_1)));
        K1(m,n)=phase1_1*phase2_1*amb_1*J;

        % for receiver_2
        arg1_2=((Y1+Z2).')*((u*((Z2.')*p))-(v*((Z2.')*x)));
        phase1_2=exp(-i*k_y*arg1_2/c);
        arg2_2=((Y1+Z1).')*((p-x)+(0.5*(u-v)*(((Y1+Z2).')*(p+x))));
        phase2_2=exp(i*k_y*arg2_2/c);
        tau_2=1/c*(((Y1+Z2).')*(p-x));
        neu_2=k_y*(((Y1+Z2).')*(u-v));
        amb_2=pi*(pulse-abs(tau_2))*exp(-
i*0.5*neu_2*pulse)*sinc((0.5/pi)*(-neu_2)*(pulse-abs(tau_2)));
        K2(m,n)=phase1_2*phase2_2*amb_2*J;

        % for receiver_3
        arg1_3=((Y1+Z3).')*((u*((Z3.')*p))-(v*((Z3.')*x)));
        phase1_3=exp(-i*k_y*arg1_3/c);
        arg2_3=((Y1+Z3).')*((p-x)+(0.5*(u-v)*(((Y1+Z3).')*(p+x))));
        phase2_3=exp(i*k_y*arg2_3/c);
        tau_3=1/c*(((Y1+Z3).')*(p-x));
        neu_3=k_y*(((Y1+Z3).')*(u-v));
        amb_3=pi*(pulse-abs(tau_3))*exp(-
i*0.5*neu_3*pulse)*sinc((0.5/pi)*(-neu_3)*(pulse-abs(tau_3)));
        K3(m,n)=phase1_3*phase2_3*amb_3*J;

        % for receiver_4
        arg1_4=((Y1+Z4).')*((u*((Z4.')*p))-(v*((Z4.')*x)));
        phase1_4=exp(-i*k_y*arg1_4/c);
        arg2_4=((Y1+Z4).')*((p-x)+(0.5*(u-v)*(((Y1+Z4).')*(p+x))));
        phase2_4=exp(i*k_y*arg2_4/c);
        tau_4=1/c*(((Y1+Z4).')*(p-x));
        neu_4=k_y*(((Y1+Z4).')*(u-v));
        amb_4=pi*(pulse-abs(tau_4))*exp(-
i*0.5*neu_4*pulse)*sinc((0.5/pi)*(-neu_4)*(pulse-abs(tau_4)));
        K4(m,n)=phase1_4*phase2_4*amb_4*J;

        % for receiver_5
        arg1_5=((Y1+Z5).')*((u*((Z5.')*p))-(v*((Z5.')*x)));
        phase1_5=exp(-i*k_y*arg1_5/c);
        arg2_5=((Y1+Z5).')*((p-x)+(0.5*(u-v)*(((Y1+Z5).')*(p+x))));
        phase2_5=exp(i*k_y*arg2_5/c);
        tau_5=1/c*(((Y1+Z5).')*(p-x));
        neu_5=k_y*(((Y1+Z5).')*(u-v));
        amb_5=pi*(pulse-abs(tau_5))*exp(-
i*0.5*neu_5*pulse)*sinc((0.5/pi)*(-neu_5)*(pulse-abs(tau_5)));
        K5(m,n)=phase1_5*phase2_5*amb_5*J;
```

```
        % for receiver_6
        arg1_6=((Y1+Z6).')*((u*((Z6.')*p))-(v*((Z6.')*x)));
        phase1_6=exp(-i*k_y*arg1_6/c);
        arg2_6=((Y1+Z6).')*((p-x)+(0.5*(u-v)*(((Y1+Z6).')*(p+x))));
        phase2_6=exp(i*k_y*arg2_6/c);
        tau_6=1/c*(((Y1+Z6).')*(p-x));
        neu_6=k_y*(((Y1+Z6).')*(u-v));
        amb_6=pi*(pulse-abs(tau_6))*exp(-
i*0.5*neu_6*pulse)*sinc((0.5/pi)*(-neu_6)*(pulse-abs(tau_6)));
        K6(m,n)=phase1_6*phase2_6*amb_6*J;

        % for receiver_7
        arg1_7=((Y1+Z7).')*((u*((Z7.')*p))-(v*((Z7.')*x)));
        phase1_7=exp(-i*k_y*arg1_7/c);
        arg2_7=((Y1+Z7).')*((p-x)+(0.5*(u-v)*(((Y1+Z7).')*(p+x))));
        phase2_7=exp(i*k_y*arg2_7/c);
        tau_7=1/c*(((Y1+Z7).')*(p-x));
        neu_7=k_y*(((Y1+Z7).')*(u-v));
        amb_7=pi*(pulse-abs(tau_7))*exp(-
i*0.5*neu_7*pulse)*sinc((0.5/pi)*(-neu_7)*(pulse-abs(tau_7)));
        K7(m,n)=phase1_7*phase2_7*amb_7*J;

        % for receiver_8
        arg1_8=((Y1+Z8).')*((u*((Z8.')*p))-(v*((Z8.')*x)));
        phase1_8=exp(-i*k_y*arg1_8/c);
        arg2_8=((Y1+Z8).')*((p-x)+(0.5*(u-v)*(((Y1+Z8).')*(p+x))));
        phase2_8=exp(i*k_y*arg2_8/c);
        tau_8=1/c*(((Y1+Z8).')*(p-x));
        neu_8=k_y*(((Y1+Z8).')*(u-v));
        amb_8=pi*(pulse-abs(tau_8))*exp(-
i*0.5*neu_8*pulse)*sinc((0.5/pi)*(-neu_8)*(pulse-abs(tau_8)));
        K8(m,n)=phase1_8*phase2_8*amb_8*J;

K(m,n)=(abs(K1(m,n)+K2(m,n)+K3(m,n)+K4(m,n)+K5(m,n)+K6(m,n)+K7(m,n)+K8(m
,n))).^2;

    end
end

%%%%%%%%%%%%%%%%
3-D Slice Plot for Position-Space
%%%%%%%%%%%%%%%%

p_x_start=-20;
p_x_end=20;
p_y_start=-20;
p_y_end=20;
p_z_start=-20;
p_z_end=20;
res_p=0.5;
p_x=p_x_start:res_p:p_x_end;   % define vector of x-axis values
p_y=p_y_start:res_p:p_y_end;   % define vector of y-axis values
p_z=p_z_start:res_p:p_z_end;

nx=length(p_x);                % length of x = columns in K
ny=length(p_y);                % length of y = rows in K
nz=length(p_z);                % length of z = pages in K
K=zeros(ny,nx,nz);             % initialize K matrix
K1=zeros(ny,nx,nz);
K2=zeros(ny,nx,nz);

for a=1:nz
    for m=1:ny
```

```
        for n=1:nx

            p=(10^3)*[p_x_start+((n-1)*res_p);p_y_end-((m-
1)*res_p);p_z_start+((a-1)*res_p)];

            % for receiver_1
            arg1_1=((Y1+Z1).')*((u*((Z1.')*p))-(v*((Z1.')*x)));
            phase1_1=exp(-i*k_y*arg1_1/c);
            arg2_1=((Y1+Z1).')*((p-x)+(0.5*(u-v)*(((Y1+Z1).')*(p+x))));
            phase2_1=exp(i*k_y*arg2_1/c);
            tau_1=1/c*(((Y1+Z1).')*(p-x));
            neu_1=k_y*(((Y1+Z1).')*(u-v));
            amb_1=pi*(pulse-abs(tau_1))*exp(-
i*0.5*neu_1*pulse)*sinc((0.5/pi)*(-neu_1)*(pulse-abs(tau_1)));
            K1(m,n,a)=phase1_1*phase2_1*amb_1*J;

            % for receiver_2
            arg1_2=((Y1+Z2).')*((u*((Z2.')*p))-(v*((Z2.')*x)));
            phase1_2=exp(-i*k_y*arg1_2/c);
            arg2_2=((Y1+Z1).')*((p-x)+(0.5*(u-v)*(((Y1+Z2).')*(p+x))));
            phase2_2=exp(i*k_y*arg2_2/c);
            tau_2=1/c*(((Y1+Z2).')*(p-x));
            neu_2=k_y*(((Y1+Z2).')*(u-v));
            amb_2=pi*(pulse-abs(tau_2))*exp(-
i*0.5*neu_2*pulse)*sinc((0.5/pi)*(-neu_2)*(pulse-abs(tau_2)));
            K2(m,n,a)=phase1_2*phase2_2*amb_2*J;

            K(m,n,a)=(abs(K1(m,n,a)+K2(m,n,a))).^2;

        end
    end
end

%%%%%%%%%%%%%%%%%
Ambiguity Implementation for Chirp Signal
%%%%%%%%%%%%%%%%%

        amb_1=pi*(pulse-abs(tau_1))*exp(i*0.5*(-
neu_1+(gamma*tau_1))*pulse)*sinc((0.5/pi)*(-neu_1+(gamma*tau_1))*(pulse-
abs(tau_1)));

%%%%%%%%%%%%%%%%%
Output Plot
%%%%%%%%%%%%%%%%%

clear all
image(p_x,p_y,64*K/max(max(K)))
hold on
plot(2,0,'+k',-5,5,'^k',15,15,'^k',-2,-15,'^k',15,-
15,'^k','linewidth',2)
hold off
xlabel({'\fontsize{11} x-component','\fontsize{11} (position)'})
ylabel({'\fontsize{11} y-component','\fontsize{11} (position)'})
title({'\fontsize{12} Transmitter/Receiver Geometry 1'})

% Slice Plot
norm=max(max(max(K)));
[UX,UY,UZ]=meshgrid(u_x,u_y,u_z);
slice(UX,UY,UZ,K/norm,[0],[0],[0])
colorbar
```

LIST OF REFERENCES

[1] B. Borden, *Radar imaging of airborne targets: A primer for applied Mathematicians and Physicists*, Taylor & Francis, 1999.

[2] M. Cheney and B. Borden, "Imaging moving targets from scattered waves," Institute of Physics Publishing on Inverse Problems, Vol. 24, April 2008.

[3] K. Tomiyasu, "Tutorial review of synthetic aperture radar (SAR) with applications to imaging of the ocean surface," Proceedings of the IEEE, Vol. 66, No. 5, pp. 563-583, May 1978.

[4] M. J. Gerry, L. C. Potter, I. J. Gupta and Andria van der Merwe, "A parametric model for synthetic aperture radar measurements," IEEE Trans Antennas and Propagation, Vol. 47, No. 7, pp. 1179-1188, July 1999.

[5] E. G. Larsson, G. Liu, P. Stocia and J. Li, "High-resolution SAR imaging with angular diversity," IEEE Trans Aerospace and Electronic Systems, Vol. 37, No. 4, pp. 1359-1372, October 2001.

[6] B. Borden and M. Cheney, "Synthetic aperture imaging from high-Doppler resolution measurements," Institute of Physics Publishing on Inverse Problems, Vol. 21, 2005.

[7] F. Berizzi, E. Dalle Mese, M. Diani and M. Martorella, "High-resolution ISAR imaging of maneuvering targets by means of the range instantaneous Doppler technique: Modeling and performance analysis," IEEE Trans Image Processing, Vol. 10, No. 12, pp. 1880-1890, December 2001.

[8] B. Zheng *et al*, "Time-frequency approaches to ISAR imaging of maneuvering targets and their limitations," IEEE Correspondence, 2001.

[9] T. Tsao, M. Slamani, P. Varshney, D. Weiner and H. Schwarzlander, "Ambiguity function for bistatic radar," IEEE Correspondence, 1997.

[10] B. Friedlander and B. Porat, "VSAR: A high resolution radar system for detection of moving targets," IEE Proc Radar, Sonar Navig., Vol. 144, No. 4, pp. 205-218, August 1997.

[11] Y. L. Wang et al., "Space-time adaptive processing for airborne radar with various array orientations," IEE Proc Radar, Sonar Navig., Vol. 144, No. 6, pp. 330-340, December 1997.

[12] B. Borden, “Mathematical problems in radar inverse scattering,” Institute of Physics Publishing on Inverse Problems, Vol. 18, No. 1, February 2002.

[13] J. B. Keller, “Inverse problems,” The American Mathematical Monthly, Vol. 83, No. 2, pp. 107-118, February 1976.

[14] M. I. Skolnik, *Introduction to radar systems*, 2nd edition, McGraw-Hill, 2001.

[15] H. D. Griffiths, “Developments in modern synthetic aperture radar,” IEEE Radar Conference, pp. 734-739, April 2007.

[16] Ausherman *et al.*, “Developments in radar imaging,” IEEE Trans Aerospace and Electronic Systems, Vol. AES-20, No. 4, pp. 363-400, July 1984.

[17] J. P. Zwart, *Aircraft recognition from features extracted from measured and simulated radar range profiles*, ASCI, The Netherlands, 2003.

[18] M. Cheney and B. Borden, *Fundamentals of radar imaging*, SIAM, 2009

[19] “Radar,” class notes for PH 4274, Physics Department, Naval Postgraduate School, May 2008.

[20] V. C. Chen, H. Ling, “Time-Frequency Transforms for radar imaging and signal analysis,” *Norwood, MA: Artech House*, 2002.

[21] S. S. Jae, G. Thomas, B. C. Flores, “Range-Doppler radar imaging and motion compensation,” *Norwood, MA: Artech House*, 2001.

[22] M. Bertero and P. Boccacci, *Introduction to inverse problems in imaging*, pp. 81-86. Institute of Physics Publishing, UK, 1998.

[23] J. R. Guerci, *Space-time adaptive processing for radar*, Artech House, 2003.

[24] J. S. Bergin and P. M. Techau, “Multiresolution signal processing techniques for ground moving target detection using radar,” EURASIP Journal on Applied Signal Processing, No. 47534, 2006.

[25] G. Y. Wang *et al.*, “Dual-speed SAR imaging of moving targets,” IEEE Trans Aerospace and Electronic Systems, Vol. 42, No. 1, pp. 368-379, January 2006.

[26] J. K. Jao, “Theory of synthetic aperture radar imaging of a moving target,” IEEE Trans GeoScience and Remote Sensing, Vol. 39, No. 9, pp. 1984-1992, September 2001.

INITIAL DISTRIBUTION LIST

1. Defense Technical Information Center
   Ft. Belvoir, Virginia

2. Dudley Knox Library
   Naval Postgraduate School
   Monterey, California

3. Professor James H. Luscombe
   Code PH/Lj
   Naval Postgraduate School
   Monterey, California

4. Professor Brett Borden
   Code PH/Bb
   Naval Postgraduate School
   Monterey, California

5. Professor Donald L. Walters
   Code PH/We
   Naval Postgraduate School
   Monterey, California

6. Professor Yeo Tat Soon
   Director, Temasek Defence Science Institute
   National University of Singapore
   Singapore

7. Tan Lai Poh (Ms)
   Assistant Manager, Temasek Defence Science Institute
   National University of Singapore
   Singapore

8. Tan Lu Pin
   Ministry of Defence
   Singapore